

Computational Science Laboratory
Report CSL-TR-21-10
April 13, 2022

Amit N Subrahmanya, Andrey A Popov,
Adrian Sandu

*“Ensemble Variational Fokker-Planck
Methods for Data Assimilation”*

Computational Science Laboratory
“Compute the Future!”

Department of Computer Science
Virginia Tech
Blacksburg, VA 24060
Phone: (540) 231-2193
Fax: (540) 231-6075

Email: amitns@vt.edu, apopov@vt.edu, sandu@vt.edu
Web: <https://csl.cs.vt.edu>



ENSEMBLE VARIATIONAL FOKKER-PLANCK METHODS FOR DATA ASSIMILATION*

AMIT N. SUBRAHMANYA [†], ANDREY A. POPOV[†], AND ADRIAN SANDU[†]

Abstract. Particle flow filters that smoothly transform particles from being samples of a prior distribution to samples of a posterior, are a major topic of active research. In this work, we introduce a generalized data assimilation framework called the Variational Fokker-Planck method for filtering and smoothing whose specific implementations are the previously known methods such as the mapping particle filter and Langevin-based filters. Using the properties of an optimal Itô process that drives the corresponding Fokker-Planck equation, we derive natural dynamics for known heuristics such as particle rejuvenation and regularization to fit into the said framework. We also extend our framework to higher dimensions using localization and covariance shrinkage, and provide a robust implicit-explicit method for evolving the Itô process, as a stochastic initial value problem. The effectiveness of the variational Fokker-Planck method is demonstrated on three incrementally challenging test problems, namely the Lorenz '63, Lorenz '96 and the quasi-geostrophic equations.

Key words. Data Assimilation, Bayesian Inference, Particle Filter

AMS subject classifications. 65C05, 93E11, 62F15, 86A22

1. Introduction. Data assimilation (DA) [5, 46] seeks to estimate the state of a physical system by optimally combining sparse and noisy observations of reality with background information obtained from a computational model of the system. As exact Bayesian inference for this state estimation problem is computationally intractable, statistical sampling methods are frequently used to perform approximate inference. These statistical methods typically suffer from the curse of dimensionality [21], and the main focus of research is computationally efficient and robust methods for high-dimensional problems.

Popular statistical methods for data assimilation include the Ensemble Kalman Filter (EnKF) [7, 15, 16] and the Ensemble Kalman Smoother (EnKS) [17] and related methods. One problem with the above methods is filter divergence. When the state variables in an ensemble start to mimic each other, the ensemble covariance becomes extremely small, and the filter trusts the model while discarding the observations – resulting in the divergence of the analysis trajectory from the truth. Popular heuristics to prevent collapse include anomaly inflation [40], and particle rejuvenation [9, 41]. In high-dimensional problems, estimates of statistics such as the covariance are inaccurate, due to a dearth of samples, requiring heuristic fixes such as localization [4] and covariance shrinkage [8].

An alternative to ensemble Kalman-like methods are particle filters [57] that make little to no assumptions about any of the involved distributions. These methods suffer from particle degeneracy, when the weight of one particle is large, and the weights of the other particles are close to zero. Resampling particles periodical is needed to recover from degeneracy. Traditional particle filters based on sequential importance with resampling [56] are infeasible for large state spaces as they require an exorbitantly large number of particles to successfully assimilate observations. More

*Submitted to the arXiv April 13, 2022.

Funding: This work was supported by DOE through award ASCR DE-SC0021313, by NSF through award CDS&E-MSS 1953113, and by the Computational Science Laboratory at Virginia Tech.

[†]Computational Science Laboratory, Department of Computer Science, Virginia Tech, Blacksburg, VA (amitns@vt.edu, apopov@vt.edu, sandu@vt.edu).

robust approaches to particle filtering such as the Ensemble Transport Particle Filter (ETPF) [2] and the Marginal Adjusted Rank Histogram Filter (MARHF) [3] have been developed.

The particle flow filtering approach [26], where particles move continuously in the state space toward samples from a posterior distribution, has attracted considerable attention recently as a general methodology for Bayesian inference. The pioneering work of Liu and Wang [33] proposed the Stein variational gradient descent method, which leverages the fact that the Stein discrepancy is equal to the gradient of the Kullback-Leibler (KL) divergence [29] between the current and the posterior distributions. This gradient is used to move particles in state space closer to a sample from the posterior distribution. A reproducing kernel Hilbert space (RKHS) embedding of the particles is used to provide a rigorous framework for the derivation, and results in a closed form solution of the gradients. A drawback of this approach is the need to choose a RKHS, and the strong dependency of the particle flow on the assumed kernel. The mapping particle filter (MPF) of Pulido and van Leeuwen [42] employs the Stein variational gradient descent approach to perform data assimilation. The aim is to progressively minimize the KL divergence between the posterior distribution and the sequence of intermediate particle distributions and the posterior distribution. The major drawback is the scalability to higher dimensions, where one needs to heuristically tune the kernels of RKHS when the number of particles are sparse. To increase robustness in high dimensions, Hu and van Leeuwen proposed the particle flow filter (PFF) [22], where different localized kernel functions are used for each state variable.

While the previously discussed approaches [22, 33, 42] view the particle flow problem through the lens of optimization, more recent work [47, 50] takes a dynamical system point of view where an Itô process evolves particles from a samples of one distribution to becoming samples of the posterior distribution. Reich and Weissmann [47] consider the dynamics of an interacting system of particles under the influence of an Itô process, and the evolution of the corresponding probability distributions via the Fokker Planck equation. They discuss sufficient conditions for the evolving probability densities to approach a steady state equal to the posterior distribution, which allows to perform Bayesian inference with a wide variety of interacting particle approximations. A major drawback of this approach is that the evolution of the interactive particle system is highly stiff, and requires expensive numerical integration approaches. A related approach is proposed Garbuno-Inigo et. al. [18] where the particle dynamics is given by interacting Langevin diffusions. The Fokker-Planck equation associated with the stochastic process has an exploitable gradient structure built on the Wasserstein metric and the covariance of the diffusion, which ensures convergence to the desired posterior distribution. A derivative-free implementation of the dynamics is proposed, which allows to extend Ensemble Kalman Inversion [25] to compute samples from a Bayesian posterior.

In this work we introduce a generalized variational Fokker-Planck (VFP) approach to data assimilation. Following the particle flow filter philosophy, a stochastic dynamical process moves particles in state space, such that the underlying probability density approaches the desired posterior in the limit of infinite time [26]. We also show that previous methods such as the MPF and the PFF are particular cases of VFP algorithms. In the VFP framework, the MPF is represented by a kernel assumption on both the prior and intermediate distributions, and PFF is represented by a Gaussian assumption on the prior and a kernel assumption on the intermediate, both with zero diffusion.

The VFP framework, though superficially similar to Reich’s Fokker-Planck [47]

idea and Langevin dynamics [18] is different in the fact that our framework uses a novel time discretization method to evolve the optimal Itô process in a stable manner, while at the same time being much less restrictive in the dynamics.

The key contributions of this paper are: (i) a generalized formulation of the variational Fokker-Planck approach aimed towards data assimilation, (ii) derivation of the optimal drift of an Itô process to minimize the Kullback-Leibler divergence between the forecast and posterior distributions, (iii) a general implementation via combinations of parameterized distributions, (iv) extension to solve smoothing problems, (v) performing localization for high dimensional problems, (vi) derivation of regularization to ensure particle diversity by minimizing the mutual information between particles, and (vii) derivation of partitioned implicit-explicit (IMEX) time stepping method to evolve the stiff Itô process in time.

The remainder of this paper is organized as follows. The general discrete time data assimilation problem is reviewed in Section 2 along with a description of notation. In Section 3, we develop the proposed variational Fokker-Planck filter, including the derivation of the optimal drift and regularization terms, options to parametrize the intermediate distributions, and implementation aspects. Numerical experiments to validate the methodology using Lorenz '63 [35, 53], Lorenz '96 [34, 55] and quasi-geostrophic equations [51] are reported in Section 7. Concluding remarks are drawn in Section 8.

2. Background. Let $\mathbf{x}_k^{\text{true}} \in \mathbb{R}^{\text{N}_{\text{state}}}$ represent the true state of a dynamical system at time t_k . We only have limited information about it, and the prior uncertainty (in our knowledge) is described by the distribution of the random variable $\mathbf{x}_k^{\text{b}} \sim \mathcal{P}_k^{\text{b}}$, called the background. Let \mathbf{y}_k denote a noisy observation of the truth at time t_k :

$$(2.1) \quad \mathbf{y}_k = \mathcal{H}_k(\mathbf{x}_k^{\text{true}}) + \varepsilon_k^{\text{obs}}, \quad \mathbf{y}_k \in \mathbb{R}^{\text{N}_{\text{state}}}, \quad k \geq 0,$$

where $\mathcal{H}_k : \mathbb{R}^{\text{N}_{\text{state}}} \rightarrow \mathbb{R}^{\text{N}_{\text{obs}}}$ is a non-linear observation operator, and $\varepsilon_k^{\text{obs}} \sim \mathcal{P}_k^{\text{obs}}$ is (a realization of) the observation error. It is assumed that the observation error distribution $\mathcal{P}_k^{\text{obs}}$ is known, and that observation errors at different times are independent of random variables. In most operational problems of interest, the observations are spatially sparse, i.e., $\text{N}_{\text{obs}} \ll \text{N}_{\text{state}}$. Our goal is to perform Bayesian inference using these two sources of information to decrease uncertainty; the improved estimate of the true state is a random variable $\mathbf{x}_k^{\text{a}} \sim \mathcal{P}_k^{\text{a}}$, called the analysis state, where the posterior (analysis) distribution

$$(2.2) \quad \mathcal{P}_k^{\text{a}}(\mathbf{x}) = \mathcal{P}_k^{\text{b}}(\mathbf{x}|\mathbf{y}_k) = \frac{\mathcal{P}_k^{\text{obs}}(\mathbf{y}_k|\mathbf{x})\mathcal{P}_k^{\text{b}}(\mathbf{x})}{\mathcal{P}_k(\mathbf{y}_k)},$$

represents the sum total of our knowledge about the state at time t_k .

By propagating the analysis forward in time from t_k to t_{k+1} :

$$(2.3) \quad \mathbf{x}_{k+1}^{\text{b}} = \mathcal{M}_{k,k+1}(\mathbf{x}_k^{\text{a}}) + \eta_k, \quad k \geq 0,$$

through the model operator $\mathcal{M}_{k+1} : \mathbb{R}^{\text{N}_{\text{state}}} \rightarrow \mathbb{R}^{\text{N}_{\text{state}}}$, a new prior is obtained at time t_{k+1} , and the cycle can begin anew. The model error term η_k is taken to be zero for the remainder of this paper, i.e., we assume a perfect model.

Consider the data assimilation window $[t_0, t_K]$. The filtering approach to the Bayesian inference problem (2.2) incorporates only the observation at the current time, and produces analyses conditioned by all past observations $\mathbf{x}_k^{\text{a}} \sim \mathcal{P}(\mathbf{x}_k^{\text{a}} | \mathbf{y}_{0:k})$

for $0 \leq k \leq K$:

(2.4)

$$\mathbf{x}_k^a \sim \mathcal{P}(\mathbf{x}_k | \mathbf{y}_{0:k}) = \frac{\mathcal{P}_k^{\text{obs}}(\mathbf{y}_k | \mathbf{x}_k)}{\mathcal{P}_k(\mathbf{y}_k)} \mathcal{P}_k(\mathbf{x}_k | \mathbf{y}_{0:k-1}) \stackrel{\eta_i=0}{=} \left[\prod_{i=0}^k \frac{\mathcal{P}_i^{\text{obs}}(\mathbf{y}_i | \mathbf{x}_i)}{\mathcal{P}_i(\mathbf{y}_i)} \right] \mathcal{P}_0^b(\mathbf{x}_0).$$

The smoothing approach incorporates all present and future observations into the current analysis,

(2.5)

$$\mathbf{x}_k^a \sim \mathcal{P}(\mathbf{x}_k | \mathbf{y}_{0:K}) = \left[\prod_{i=k}^K \frac{\mathcal{P}_i^{\text{obs}}(\mathbf{y}_i | \mathbf{x}_k)}{\mathcal{P}_i(\mathbf{y}_i)} \right] \mathcal{P}_k^b(\mathbf{x}_k) \stackrel{\eta_i=0}{=} \left[\prod_{i=0}^K \frac{\mathcal{P}_i^{\text{obs}}(\mathbf{y}_i | \mathbf{x}_i)}{\mathcal{P}_i(\mathbf{y}_i)} \right] \mathcal{P}_0^b(\mathbf{x}_0).$$

In practice, performing exact Bayesian inference (2.4) or (2.5) is computationally infeasible. Computationally tractable algorithms are obtained via sampling-based or Monte-Carlo approaches that represent the probability densities used in inference (2.2) by their empirical counterparts. Consider an ensemble of N_{ens} realizations (or samples) of the random variable $\mathbf{x} \sim \mathcal{P}$,

$$(2.6) \quad \mathbf{X} := [\mathbf{x}^{[1]}, \mathbf{x}^{[2]}, \dots, \mathbf{x}^{[N_{\text{ens}}]}] \in \mathbb{R}^{N_{\text{state}} \times N_{\text{ens}}}.$$

In the ensemble limit of $N_{\text{ens}} \rightarrow \infty$, the empirical measure distribution of the ensemble,

$$(2.7) \quad \tilde{\mathcal{P}}(\mathbf{x}) = \frac{1}{N_{\text{ens}}} \sum_{i=1}^{N_{\text{ens}}} \delta_{\mathbf{x}^{[i]}}(\mathbf{x}),$$

converges weakly almost surely to the distribution of the random variable $\mathcal{P}(\mathbf{x})$. When the random variable \mathbf{x} describes the state of a dynamical system, each ensemble member $\mathbf{x}^{[e]}$ is called a particle to hint at its propagation in time. We use this convention for the remainder of this paper.

Particles are used to estimate statistics of the probability distribution \mathcal{P} . For example, the empirical mean and covariance are defined as

$$(2.8) \quad \bar{\mathbf{x}} = \frac{1}{N_{\text{ens}}} \mathbf{X} \mathbf{1}_{N_{\text{ens}}}, \quad \mathbf{P} = \mathbf{A} \mathbf{A}^T \quad \text{with} \quad \mathbf{A} = \frac{1}{\sqrt{N_{\text{ens}} - 1}} (\mathbf{X} - \bar{\mathbf{x}} \mathbf{1}_{N_{\text{ens}}}^T),$$

respectively, where $\mathbf{1}_p$ represents a p -dimensional vector of ones.

3. The Variational Fokker-Planck approach to data assimilation. Ensemble based data assimilation methods represent probability densities by their empirical counterparts (2.6). For the remainder of this paper we ignore the physical time subscripts k for data assimilation: $\mathbf{x}^b \equiv \mathbf{x}_k^b$, $\mathcal{P}^b \equiv \mathcal{P}_k^b$, $\mathbf{x}^a \equiv \mathbf{x}_k^a$, $\mathcal{P}^a \equiv \mathcal{P}_k^a$. The background probability density is represented by a background ensemble of particles $\mathbf{X}^b = [\mathbf{x}^{b[1]}, \dots, \mathbf{x}^{b[N_{\text{ens}}]}]$ with $\mathbf{x}^{b[e]} \sim \mathcal{P}^b(\mathbf{x})$. The filter seeks to produce an analysis ensemble $\mathbf{X}^a = [\mathbf{x}^{a[1]}, \dots, \mathbf{x}^{a[N_{\text{ens}}]}]$ with $\mathbf{x}^{a[e]} \sim \mathcal{P}^a(\mathbf{x})$ that represents the analysis probability density. In EnKF and its various flavors, the analysis ensemble is obtained in a single (non-iterative) step by combining the background ensemble and observations under Gaussian assumptions. In traditional particle filters, rather than modifying particles, the weight associated with each particle is modified. The analysis involves combining the background weights with the observation likelihoods to obtain the analysis weights.

Particle flow filters use a dynamical system approach to transform a set of Monte Carlo samples $\mathbf{x}^{b[e]}$ from the prior distribution into samples $\mathbf{x}^{a[e]}$ from the posterior

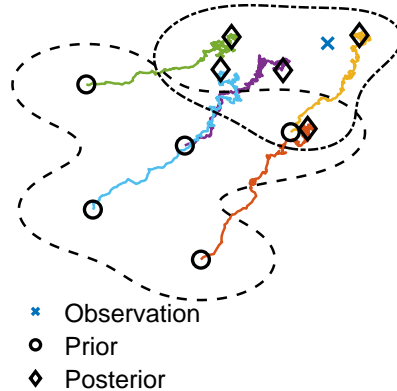


Fig. 3.1: Flow of particles sampled from a prior distribution to samples from the posterior distribution. The particles move under the flow of a stochastic differential equation.

distribution [6,12,18,26,47,52]. Particles move in state space according to an evolution equation in artificial time τ , and the corresponding probability distributions evolve accordingly.

Two approaches to moving the particles have been proposed. One approach formulates a flow over a finite time interval $\tau \in [0, 1]$, starts with the prior distribution at $\tau = 0$, and reaches the posterior distribution at $\tau = 1$ [45]. A second approach formulates a flow over the finite time interval $\tau \in [0, \infty)$, and maps any initial distribution to the posterior distribution asymptotically when $\tau \rightarrow \infty$. Examples of such filters include the Stein variational gradient descent [32,33], the mapping particle filter [22,43], interacting Langevin diffusions [18], and Fokker-Planck particle systems [47]. In this work we generalize these methods and propose the Variational Fokker-Planck (VFP) approach to data assimilation.

The main idea is as follows. The initial configuration of the system is a set of particles drawn from the prior distribution $\mathbf{x}^{b[e]} \sim \mathcal{P}^b$. The particles move – in artificial time – under the flow of an Itô process, and the distribution of the particles evolves according to the corresponding Fokker-Planck equation [29]. The flow is defined such as to push the particles toward samples from the posterior distribution $\mathbf{x}^{a[e]} \sim \mathcal{P}^a$.

This idea is illustrated in Figure 3.1. The prior/background particles are depicted by the circles whose density is shown by the dashed line. These particles flow towards the observation under an optimal Itô process depicted by colored lines. The final analysis positions of the particles are given by the diamond, with the dash-dotted line around the analysis particles represent the posterior distribution.

3.1. Derivation of the optimal drift. A general initial value Itô process that acts on a random variable $\mathbf{x}_\tau \in \mathbb{R}^{N_{\text{state}}}$ is [14,28]

$$(3.1) \quad d\mathbf{x}_\tau = \mathbf{F}(\tau, \mathbf{x}_\tau) d\tau + \boldsymbol{\sigma}(\tau, \mathbf{x}_\tau) d\mathbf{W}_\tau, \quad \tau \geq 0,$$

where $\mathbf{F} : \mathbb{R}_+ \times \mathbb{R}^{N_{\text{state}}} \rightarrow \mathbb{R}^{N_{\text{state}}}$ is the drift term, $\boldsymbol{\sigma} : \mathbb{R}_+ \times \mathbb{R}^{N_{\text{state}}} \rightarrow \mathbb{R}^{N_{\text{state}} \times M}$ is the diffusion matrix, $\mathbf{W}_\tau \in \mathbb{R}^M$ is an M -dimensional standard Wiener process. Here, the subscript τ represents the synthetic time of the Itô process (3.1). The random variables at each synthetic time τ have a probability density $\mathbf{x}_\tau \sim q_\tau(\mathbf{x})$.

The Fokker-Planck equation [29] representing the evolution of the probability density $q_\tau(\mathbf{x})$ under (3.1) is:

$$(3.2) \quad \frac{\partial q_\tau(\mathbf{x})}{\partial \tau} = - \sum_{i=1}^{N_{\text{state}}} \frac{\partial}{\partial \mathbf{x}_i} (q_\tau(\mathbf{x}) \mathbf{F}_i(\tau, \mathbf{x})) + \sum_{i=1}^{N_{\text{state}}} \sum_{j=1}^{N_{\text{state}}} \frac{\partial^2}{\partial \mathbf{x}_i \partial \mathbf{x}_j} (q_\tau(\mathbf{x}) \mathbf{D}_{i,j}(\tau, \mathbf{x})),$$

where $\mathbf{D}(\tau, \mathbf{x}) := \frac{1}{2} \boldsymbol{\sigma}(\tau, \mathbf{x}) \boldsymbol{\sigma}^T(\tau, \mathbf{x}) \in \mathbb{R}^{N_{\text{state}} \times N_{\text{state}}}$ is the defined diffusion tensor. For the sake of future calculations, equation (3.2) is rewritten as

$$(3.3) \quad \frac{\partial q_\tau(\mathbf{x})}{\partial \tau} = - \operatorname{div} (q_\tau(\mathbf{x}) [\mathbf{F}(\tau, \mathbf{x}) - \mathbf{D}(\tau, \mathbf{x}) \nabla_{\mathbf{x}} \log q_\tau(\mathbf{x}) - \mathbf{d}(\tau, \mathbf{x})]),$$

where $\operatorname{div}(\cdot)$ is the divergence operator and $\mathbf{d}(\tau, \mathbf{x}) = \operatorname{div} \mathbf{D}(\tau, \mathbf{x}) \in \mathbb{R}^{N_{\text{state}}}$. The KL divergence [31] between $q_\tau(\mathbf{x})$ and a target $p(\mathbf{x})$ is defined as

$$(3.4) \quad D_{\text{KL}}(q_\tau \| p) = \int_{\Omega} q_\tau(\mathbf{x}) \log \frac{q_\tau(\mathbf{x})}{p(\mathbf{x})} d\mathbf{x},$$

where $\operatorname{support}(q_\tau) \subseteq \operatorname{support}(p) := \Omega$. We wish to obtain an indexed family of intermediate random variables $\{\mathbf{x}_\tau\}_{0 \leq \tau < \infty}$ that represent the particle in transition to the target. We require that the distribution of these random variables converge to the target probability distribution, in the sense that

$$(3.5) \quad \lim_{\tau \rightarrow \infty} D_{\text{KL}}(q_\tau \| p) = 0.$$

Following [33], we initialize the Itô process (3.1) with the background random variable: $\mathbf{x}_0 = \mathbf{x}^b \sim q_0(\mathbf{x}) = \mathcal{P}^b(\mathbf{x})$. The target is the posterior probability density $p(\mathbf{x}) = \mathcal{P}^a(\mathbf{x})$. We seek to find the drift term $\mathbf{F}(\tau, \mathbf{x})$ such that the family of intermediate probability densities converges in KL-divergence to posterior, $q_\infty(\mathbf{x}) = p(\mathbf{x}) = \mathcal{P}^a(\mathbf{x})$.

Consider a smooth function $\mathcal{A} : \Omega \subseteq \mathbb{R}^{N_{\text{state}}} \rightarrow \mathbb{R}^{N_{\text{state}} \times N_{\text{state}}}$ that maps each point in the domain to a positive definite matrix $\mathcal{A}(\mathbf{x})$, the space of functions of finite second order scaled moments with respect to the probability density $q(\cdot)$ over Ω , and define the following dot-product:

$$(3.6a) \quad L_{2,q,\mathcal{A}}(\Omega) = \left\{ f : \Omega \rightarrow \mathbb{R}^{N_{\text{state}}} \mid \int_{\Omega} q(\mathbf{x}) \|\mathcal{A}^{1/2}(\mathbf{x}) f(\mathbf{x})\|^2 d\mathbf{x} < \infty \right\},$$

$$(3.6b) \quad \langle f, g \rangle_{\mathcal{A}} = \int_{\Omega} q(\mathbf{x}) f^T(\mathbf{x}) \mathcal{A}(\mathbf{x}) g(\mathbf{x}) d\mathbf{x}, \quad f, g \in L_{2,q,\mathcal{A}}(\Omega).$$

THEOREM 3.1. *Consider the Itô process (3.1), and $\tau \mapsto \mathcal{A}_\tau \in \mathbb{R}^{N_{\text{state}} \times N_{\text{state}}}$ a smooth function that maps time to specified positive definite matrices. The instantaneous optimal drift $\mathbf{F}(\tau, \mathbf{x})$ that minimizes the KL-divergence (3.4) of the family of distributions governed by the Fokker-Planck equation (3.2) with respect to the dot-product $\langle \cdot, \cdot \rangle_{\mathcal{A}_\tau^{-1}}$ (3.6b) is given by:*

$$(3.7) \quad \mathbf{F}(\tau, \mathbf{x}) = \mathcal{A}_\tau \nabla_{\mathbf{x}} \log \mathcal{P}^a(\mathbf{x}) + (\mathbf{D}(\tau, \mathbf{x}) - \mathcal{A}_\tau) \nabla_{\mathbf{x}} \log q_\tau(\mathbf{x}) + \mathbf{d}(\tau, \mathbf{x}),$$

under the assumption that for all τ , $\operatorname{support}(q_\tau) \subseteq \operatorname{support}(\mathcal{P}^a) := \Omega$. The optimal drift depends on the current density q_τ , and it depends on diffusion term $\boldsymbol{\sigma}(\tau, \mathbf{x})$ via $\mathbf{D}(\tau, \mathbf{x})$ and $\mathbf{d}(\tau, \mathbf{x})$.

The Fokker-Planck equation (3.2) under the optimal drift (3.7) is given by

$$(3.8) \quad \frac{\partial q_\tau(\mathbf{x})}{\partial \tau} = -\operatorname{div} \left(q_\tau(\mathbf{x}) \mathcal{A}_\tau \nabla_{\mathbf{x}} \log \frac{\mathcal{P}^a(\mathbf{x})}{q_\tau(\mathbf{x})} \right),$$

and does not depend on the choice of the diffusion term $\boldsymbol{\sigma}(\tau, \mathbf{x})$.

Proof. We omit all explicit arguments of the probability distributions and functions for brevity. The time derivative of the KL-divergence (3.4) between q_τ and \mathcal{P}^a is given by:

$$\frac{dD_{\text{KL}}}{d\tau} = \int_{\Omega} \frac{\partial q_\tau}{\partial \tau} \left(\log \frac{q_\tau}{\mathcal{P}^a} + 1 \right) d\mathbf{x},$$

and applying the Fokker-Planck equation (3.2) leads to:

$$\frac{dD_{\text{KL}}}{d\tau} = \int_{\Omega} -\operatorname{div} \left(q_\tau (\mathbf{F} - \mathbf{D} \nabla_{\mathbf{x}} \log q_\tau - \mathbf{d}) \right) \left(\log \frac{q_\tau}{\mathcal{P}^a} + 1 \right) d\mathbf{x}.$$

Assuming $q_\tau|_{\partial\Omega} = 0$, integrating by parts, and using (3.6b) leads to:

$$\begin{aligned} \frac{dD_{\text{KL}}}{d\tau} &= \int_{\Omega} q_\tau (\mathbf{F} - \mathbf{D} \nabla_{\mathbf{x}} \log q_\tau - \mathbf{d})^T \nabla_{\mathbf{x}} \left(\log \frac{q_\tau}{\mathcal{P}^a} \right) d\mathbf{x} \\ &= \left\langle \mathbf{F} - \mathbf{D} \nabla_{\mathbf{x}} \log q_\tau - \mathbf{d}, \mathcal{A}_\tau \nabla_{\mathbf{x}} \left(\log \frac{q_\tau}{\mathcal{P}^a} \right) \right\rangle_{\mathcal{A}_\tau^{-1}}. \end{aligned}$$

Consequently the optimal drift \mathbf{F} that maximizes the decrease of the KL-divergence with respect to \mathcal{A}_τ is given by:

$$\mathbf{F} - \mathbf{D} \nabla_{\mathbf{x}} \log q_\tau - \mathbf{d} = -\mathcal{A}_\tau \nabla_{\mathbf{x}} \left(\log \frac{q_\tau}{\mathcal{P}^a} \right),$$

as claimed in (3.7). \square

REMARK 1. The optimal drift (3.7) consists of two terms, i.e., two forces acting on the particles. The term

$$(3.9) \quad \mathcal{A}_\tau \left(\nabla_{\mathbf{x}} \log \mathcal{P}^a(\mathbf{x}) - \nabla_{\mathbf{x}} \log q_\tau(\mathbf{x}) \right)$$

is the scaled difference between the gradients log-likelihoods of the posterior and the intermediate distribution, and ensures that the intermediate distribution is pushed toward the posterior one. The term

$$(3.10) \quad \mathbf{D}(\tau, \mathbf{x}) \nabla_{\mathbf{x}} \log q_\tau(\mathbf{x}) + \operatorname{div} \mathbf{D}(\tau, \mathbf{x}),$$

is a dampening of the stochastic term $\boldsymbol{\sigma}(\tau, \mathbf{x})d\mathbf{W}_\tau$ of the Itô process (3.1), ensuring that the perturbations to any one realization of intermediate variables still move towards being a realization of the analysis.

A deterministic dynamics is obtained by setting the diffusion to zero, $\boldsymbol{\sigma} = 0$. In this case the dampening force (3.10) is zero, and the optimal drift is given by the first term (3.9). The deterministic choice does not change the optimal Fokker-Planck dynamics (3.8).

REMARK 2. The optimal drift (3.7) depends on the choice of \mathcal{A}_τ , i.e., depends on the metric in which the minimum KL-divergence tendency is measured.

1. The trivial choice, used in this paper, has $\mathcal{A}_\tau = \mathbf{I}_{N_{\text{state}}}$ giving

$$(3.11) \quad \mathbf{F}(\tau, \mathbf{x}) = \nabla_{\mathbf{x}} \log \mathcal{P}^{\text{a}}(\mathbf{x}) + (\mathbf{D}(\tau, \mathbf{x}) - \mathbf{I}_{N_{\text{state}}}) \nabla_{\mathbf{x}} \log q_\tau(\mathbf{x}) + \mathbf{d}(\tau, \mathbf{x}).$$

The space (3.6a) are functions with finite second order moments.

2. In Stein variational gradient descent [42] one chooses $\mathcal{A}_\tau = q_\tau(\mathbf{x}) \mathbf{I}_{N_{\text{state}}}$ and $\boldsymbol{\sigma}(\tau, \mathbf{x}) = 0$, giving

$$(3.12) \quad \mathbf{F}(\tau, \mathbf{x}) = q_\tau(\mathbf{x}) \nabla_{\mathbf{x}} \log \mathcal{P}^{\text{a}}(\mathbf{x}) - q_\tau(\mathbf{x}) \nabla_{\mathbf{x}} \log q_\tau(\mathbf{x}).$$

The space (3.6a) is $L_2(\Omega)$, the space of square integrable functions with respect to Lebesgue measure. Equation (3.12) can be seen as a scaling of the gradients obtained in (3.11) without stochastic noise. It would be interesting to explore the Stein choice of \mathcal{A}_τ with a non-zero $\boldsymbol{\sigma}(\tau, \mathbf{x})$, which is beyond the scope of this paper.

3. The choice $\mathcal{A}_\tau = \mathbf{D}(\tau, \mathbf{x})$ leads to Langevin dynamics [18, 37]:

$$(3.13) \quad \mathbf{F}(\tau, \mathbf{x}) = \mathbf{D}(\tau, \mathbf{x}) \nabla_{\mathbf{x}} \log \mathcal{P}^{\text{a}}(\mathbf{x}) + \mathbf{d}(\tau, \mathbf{x}),$$

and is optimal under the assumption that $\mathbf{D}(\tau, \mathbf{x})$ has full rank. If $M = N_{\text{state}}$ and the drift matrix $\boldsymbol{\sigma}(\tau, \mathbf{x}_\tau)$ in (3.1) is nonsingular, then the space (3.6a) consists of functions f for which $\boldsymbol{\sigma}^{-1} f$ has finite second order moments.

In the Langevin choice the optimal drift (3.13) does not depend on the current probability density $q_\tau(\mathbf{x})$, and therefore it allows for an efficient computation. The particles are forced apart by diffusion only.

3.2. Discretization and parameterization of the optimal drift in the VFP filter. We now discuss the discretization of the particle flow method discussed in [Section 3.1](#) using a finite number of particles. Consider an ensemble of particles $\mathbf{X}_\tau \in \mathbb{R}^{N_{\text{state}} \times N_{\text{ens}}}$ (2.6) consisting of N_{ens} samples $\mathbf{x}_\tau^{[e]} \sim q_\tau(\cdot)$. The Itô process (3.1) acts on each particle at pseudo time τ as follows:

$$(3.14) \quad d\mathbf{x}_\tau^{[e]} = \mathbf{F}(\tau, \mathbf{x}_\tau^{[e]}) d\tau + \boldsymbol{\sigma}(\tau, \mathbf{x}_\tau^{[e]}) d\mathbf{W}_\tau, \quad \mathbf{x}_0^{[e]} = \mathbf{x}^{\text{b}[e]}, \quad e = 1, \dots, N_{\text{ens}}.$$

The optimal drift (3.11) defined in [Theorem 3.1](#) acting on each particle (3.14) is:

$$(3.15) \quad \mathbf{F}(\tau, \mathbf{x}_\tau^{[e]}) = \nabla_{\mathbf{x}} \log \mathcal{P}^{\text{a}}(\mathbf{x}_\tau^{[e]}) + (\mathbf{D}(\tau, \mathbf{x}_\tau^{[e]}) - \mathbf{I}_{N_{\text{state}}}) \nabla_{\mathbf{x}} \log q_\tau(\mathbf{x}_\tau^{[e]}) + \mathbf{d}(\tau, \mathbf{x}_\tau^{[e]}),$$

and depends both on the (continuous) analysis distribution \mathcal{P}^{a} and on the (continuous) intermediate distributions q_τ , evaluated at the current particle state. We estimate these distributions at each pseudo-time τ using the ensembles \mathbf{X}^{b} and \mathbf{X}_τ , and advance the flow (3.15) using a numerical integration scheme. Under the action of the flow, \mathbf{X}_τ evolves toward an ensemble $\mathbf{X}_\infty = \mathbf{X}^{\text{a}}$ of samples from the posterior distribution \mathcal{P}^{a} given by (2.2) or (2.5).

The drift term (3.15) requires the gradient-log-likelihoods of the intermediate $q_\tau(\mathbf{x})$ and the posterior $\mathcal{P}^{\text{a}}(\mathbf{x})$ probability densities. There are two possible approaches to estimate them from the ensembles \mathbf{X}^{b} and \mathbf{X}_τ :

1. The first approach, proposed by Maoutsa et al [36], expresses each analytical gradient-log-density $-\nabla_{\mathbf{x}} \log q_\tau(\mathbf{x})$ and $-\nabla_{\mathbf{x}} \log \mathcal{P}^{\text{a}}(\mathbf{x})$ as the solution of a minimization problem; each problem is discretized using the ensembles, and the gradient-log-density values for each particle are obtained by solving a discrete optimization problem.

Mixture	$\mathcal{P}(\mathbf{x}; \Theta_{1:m}(\mathbf{x})) \propto \sum_{i=1}^m w_i \mathcal{P}_i(\mathbf{x}; \Theta_i(\mathbf{x})),$ $\nabla_{\mathbf{x}} \log \mathcal{P}(\mathbf{x}; \Theta_{1:m}(\mathbf{x})) = \frac{\sum_{i=1}^m w_i \left(\frac{\partial}{\partial \mathbf{x}} \mathcal{P}_i(\mathbf{x}; \Theta_i(\mathbf{x})) + \frac{\partial}{\partial \Theta_i} \mathcal{P}_i(\mathbf{x}; \Theta_i(\mathbf{x})) \frac{\partial \Theta_i}{\partial \mathbf{x}} \right)}{\sum_{i=1}^m w_i \mathcal{P}_i(\mathbf{x}; \Theta_i(\mathbf{x}))},$ <p>Simplifying assumption: $\partial \Theta_i / \partial \mathbf{x} = 0, \forall i$.</p>
Kernel (K)	$\mathcal{P}(\mathbf{x}) \propto \frac{1}{N_{\text{ens}}} \sum_{i=1}^{N_{\text{ens}}} \mathcal{K}(\mathbf{x} - \mathbf{x}_i),$ $\nabla_{\mathbf{x}} \log \mathcal{P}(\mathbf{x}) = \frac{\sum_i^N \nabla_{\mathbf{x}} \mathcal{K}(\mathbf{x} - \mathbf{x}_i)}{\sum_i^N \mathcal{K}(\mathbf{x} - \mathbf{x}_i)},$ <p>\mathcal{K} is a positive definite kernel function.</p>
Gaussian (G)	$\mathcal{P}(\mathbf{x}) \propto \exp(-\frac{1}{2}(\mathbf{x} - \bar{\mathbf{x}})^T \mathbf{P}^{-1} (\mathbf{x} - \bar{\mathbf{x}})),$ $\nabla_{\mathbf{x}} \log \mathcal{P}(\mathbf{x}) = -\mathbf{P}^{-1} (\mathbf{x} - \bar{\mathbf{x}}).$
Laplace (L)	$\mathcal{P}(\mathbf{x}) \propto (\theta^\nu) \mathcal{K}_\nu(\theta),$ $\nabla_{\mathbf{x}} \log \mathcal{P}(\mathbf{x}) = -\frac{2}{\theta} \frac{\mathcal{K}_{\nu-1}(\theta)}{\mathcal{K}_\nu(\theta)} \mathbf{P}^{-1} (\mathbf{x} - \bar{\mathbf{x}}),$ $\theta = \sqrt{2(\mathbf{x} - \bar{\mathbf{x}})^T \mathbf{P}^{-1} (\mathbf{x} - \bar{\mathbf{x}})}, \quad \nu = 1 - N_{\text{state}}/2,$ <p>\mathcal{K}_ν is the modified Bessel function of the second kind [1, 30].</p>
Huber (H)	<p>Huber assumption on the Laplace distribution,</p> $\nabla_{\mathbf{x}} \log \mathcal{P}(\mathbf{x}) = \begin{cases} -\delta_1 \frac{2}{\theta} \frac{\mathcal{K}_{\nu-1}(\theta)}{\mathcal{K}_\nu(\theta)} \mathbf{P}^{-1} (\mathbf{x} - \bar{\mathbf{x}}) & \delta_1 \frac{2}{\theta} \frac{\mathcal{K}_{\nu-1}(\theta)}{\mathcal{K}_\nu(\theta)} < \delta_2, \\ -\delta_2 \mathbf{P}^{-1} (\mathbf{x} - \bar{\mathbf{x}}) & \text{otherwise.} \end{cases}$
Cauchy (C)	$\mathcal{P}(\mathbf{x}) \propto (1 + (\mathbf{x} - \bar{\mathbf{x}})^T \mathbf{P}^{-1} (\mathbf{x} - \bar{\mathbf{x}}))^{-\frac{N_{\text{state}}+1}{2}},$ $\nabla_{\mathbf{x}} \log \mathcal{P}(\mathbf{x}) = -\frac{N_{\text{state}}+1}{1+(\mathbf{x}-\bar{\mathbf{x}})^T \mathbf{P}^{-1} (\mathbf{x}-\bar{\mathbf{x}})} \mathbf{P}^{-1} (\mathbf{x} - \bar{\mathbf{x}}).$

Table 3.1: A collection of several parametrized probability distributions considered in this work, and the corresponding gradient-log-densities. The letters in the parentheses represent abbreviations of the distributions used to name the various families of VFP methods. For most of the distributions listed, the parameters are a semblance of centering $\bar{\mathbf{x}} \in \mathbb{R}^{N_{\text{state}}}$ (which may, but does not necessarily stand for the mean), and a semblance of spread $\mathbf{P} \in \mathbb{R}^{N_{\text{state}} \times N_{\text{state}}}$ (which may, but does not necessarily stand for covariance).

2. The second approach, employed in this paper, reconstructs the continuous probability densities $q_\tau(\mathbf{x})$ and $\mathcal{P}^a(\mathbf{x})$ from the ensembles \mathbf{X}^b , \mathbf{X}_τ , under appropriate assumptions, computes the corresponding gradient-log-densities, and evaluates them for each particle.

To reconstruct continuous probability densities from ensembles we consider various assumptions on the form of the distributions $q_\tau(\mathbf{x})$, $\mathcal{P}^b(\mathbf{x})$, $\mathcal{P}^a(\mathbf{x})$, along with different parameterizations. Maximum likelihood values of the parameters are obtained from fitting the ensembles to the assumed distributions. For example, the intermediate density $q_\tau(\mathbf{x})$ could be assumed Gaussian in form, with parameters the mean $\bar{\mathbf{x}}_\tau$ and covariance \mathbf{P}_τ of the intermediate ensemble \mathbf{X}_τ . Different probability densities can use different assumptions.

Table 3.1 provides a non-exhaustive list of parameterized families of distributions:

- A very general approach to parametrized distributions involves mixture modeling with an arbitrary set of parameters. It is not specifically implemented in this work.
- The multivariate Gaussian distribution is an assumption similar to that made in ensemble Kalman filter methods.
- The multivariate Laplace distribution can be thought of through the lens of robust statistics [44]. The problem with the multivariate Laplace assumption is the discontinuity of the gradient at the mean. For this purpose, we build a Laplace-Gauss hybrid called the Huber distribution, which essentially makes the distribution Gaussian near the mean and Laplace at the tails. δ_1 and δ_2 are design parameters to control the relative sizes of the Laplace and Gaussian regions.
- The kernel parametrization is used in the reinterpretation of the mapping particle filter [42] and the high-dimensional flow filter [22] in the Fokker-Planck framework. Specifically, the mapping particle filter [42] is seen as a kernel parametrization on both $q_\tau(\mathbf{x})$ and $\mathcal{P}^b(\mathbf{x})$, and the high-dimensional flow filter [22] is seen as a kernel parametrization of $q_\tau(\mathbf{x})$ and a Gaussian parametrization of $\mathcal{P}^b(\mathbf{x})$.

The VFP filter computes the optimal drift (3.15) as follows:

1. Assume the form of the prior distribution $\mathcal{P}^b(\mathbf{x})$, and fit the parameters of this distribution using the background ensemble \mathbf{X}^b . Compute the corresponding negative gradient-log-likelihood function $-\nabla_{\mathbf{x}} \log \mathcal{P}^b(\mathbf{x})$.
2. By Bayes' rule (2.2) the analysis gradient-log-likelihood is the sum of the gradient-log-likelihoods of the prior distribution and of the observation distribution:

$$(3.16) \quad -\nabla_{\mathbf{x}} \log \mathcal{P}^a(\mathbf{x}) = -\nabla_{\mathbf{x}} \log \mathcal{P}^b(\mathbf{x}) - \nabla_{\mathbf{x}} \log \mathcal{P}^{\text{obs}}(\mathbf{x}).$$

The observation term is known from the (given) probability distribution of observation errors.

3. Assume the form of the intermediate probability density $q_\tau(\mathbf{x})$, and fit the parameters of this distribution using the current ensemble data \mathbf{X}_τ . Compute the corresponding negative gradient-log-likelihood function $-\nabla_{\mathbf{x}} \log q_\tau(\mathbf{x})$.
4. Compute the optimal drift via formula (3.15) by evaluating the above gradients at particle states.

The assumptions on the form of the prior distribution \mathcal{P}^b and of the intermediate distribution q_τ can differ from each other. These choices dictate the parameterization of the method. We use the abbreviations in Table 3.1 to distinguish between them. For instance, we use the notation VFP(GH) to indicate a Gaussian assumption on the prior distribution and a Huber assumption on the intermediate family. VFPLang(G) is used to denote the Langevin variant of the Fokker-Planck dynamics with a Gaussian assumption on the prior.

REMARK 3. *In this notation, the mapping particle filter [42] is reformulated as VFP(KK) where both the prior and intermediate distributions are assumed to be kernels and the high dimensional flow filter [22] is reformulated as VFP(GK) where the prior is a Gaussian distribution and the intermediate is a kernel.*

REMARK 4. *It is possible that the choices of parameterized families lead us to intermediate distributions that do not converge in KL-divergence to the analysis (3.4). For example, if \mathcal{P}^a is the product of a Gaussian (\mathcal{P}^{obs}) and Laplace (\mathcal{P}^b), then neither*

a pure Gaussian nor a pure Laplace is a good assumption on q_τ . Thus, the KL divergence between q_τ and \mathcal{P}^a can then never be zero. If we consider the parameterized family of intermediate distributions \mathcal{Q} , then, instead of seeking a distribution such that the KL-divergence is zero like in (3.5), we instead aim to solve the following problem:

$$\lim_{\tau \rightarrow \infty} \text{D}_{\text{KL}}(q_\tau \| \mathcal{P}^a) = \min_{q \in \mathcal{Q}} \text{D}_{\text{KL}}(q \| \mathcal{P}^a),$$

where we find the optimal analysis from the intermediate family that simply minimizes the KL-divergence.

3.3. Optimal drift in the VFP smoother. The optimal drift formulation (3.16) is valid for the filtering setting (2.4). We now consider the smoothing setting (2.5) for a perfect model (2.3) with $\eta_i = 0$ where $\mathbf{x}_i = \mathcal{M}_{0,i}(\mathbf{x}_0)$ for any time t_i . The entire trajectory is completely determined by the initial condition. We perform data assimilation in the space of initial conditions. The analysis probability density is:

$$(3.17) \quad \mathcal{P}^a(\mathbf{x}_0) \equiv \mathcal{P}(\mathbf{x}_0 | \mathbf{y}_{0:K}) \stackrel{\eta_i=0}{=} \left[\prod_{i=0}^K \frac{\mathcal{P}_i^{\text{obs}}(\mathbf{y}_i | \mathcal{M}_{0,i}(\mathbf{x}_0))}{\mathcal{P}_i(\mathbf{y}_i)} \right] \mathcal{P}^b(\mathbf{x}_0),$$

and the corresponding gradient log-likelihood reads:

$$(3.18) \quad -\nabla_{\mathbf{x}_0} \log \mathcal{P}^a(\mathbf{x}_0) = -\nabla_{\mathbf{x}_0} \log \mathcal{P}^b(\mathbf{x}_0) - \sum_{i=0}^K \mathbf{M}_{0:i}^*(\mathbf{x}_0) \nabla_{\mathbf{x}_i} \log \mathcal{P}_i^{\text{obs}}(\mathbf{y}_i | \mathbf{x}_i) \Big|_{\mathbf{x}_i = \mathcal{M}_{0,i}(\mathbf{x}_0)},$$

where the adjoint model operator is defined as:

$$(3.19) \quad \mathbf{M}_{0:i}^*(\mathbf{x}_0) := (\text{d}\mathcal{M}_{0,i}(\mathbf{x}_0)/\text{d}\mathbf{x}_0)^\text{T}.$$

The ensemble of particles $\mathbf{X}_\tau \in \mathbb{R}^{\text{N}_{\text{state}} \times \text{N}_{\text{ens}}}$ (2.6) consists of N_{ens} initial conditions $\mathbf{x}_{0,\tau}^{[e]} \sim q_\tau(\mathbf{x}_0)$. Each particle evolves in synthetic time τ according to the flow of the Itô process (3.14). To compute the optimal drift (3.15) a parametric approximation of $q_\tau(\cdot)$, and the corresponding gradient-log-density $\nabla_{\mathbf{x}} \log q_\tau(\cdot)$, are constructed as in the filtering case. From each initial condition one runs a full model trajectory forward in time to obtain $\mathbf{x}_{i,\tau}^{[e]} = \mathcal{M}_{0,i}(\mathbf{x}_{0,\tau}^{[e]})$ for all physical times $i = 0, \dots, K$. Next, one runs an adjoint model trajectory backward in time to compute the posterior gradient-log-density $\nabla_{\mathbf{x}_0} \log \mathcal{P}^a(\mathbf{x}_{0,\tau}^{[e]})$ (3.18). For VFP smoothing the computation of the optimal drift at each synthetic time τ requires running an ensemble of N_{ens} forward model runs, followed by N_{ens} adjoint model runs, each corresponding to a different initial condition $\mathbf{x}_{0,\tau}^{[e]}$.

3.4. Selection of the diffusion term. To complete the description of the stochastic dynamics (3.14) one needs to select the diffusion term $\boldsymbol{\sigma}(\tau, \mathbf{x})$. Recall that the optimal drift (3.7) depends on the diffusion term, however the resulting Fokker-Planck equation (3.8) does not. Nevertheless, the choice of $\boldsymbol{\sigma}(\tau, \mathbf{x})$ does impact the practical implementation of the algorithm, as well as its practical performance, given the finite number of particles and the different approximations made when reconstructing probability densities.

The trivial choice $\boldsymbol{\sigma}(\tau, \mathbf{x}) \equiv 0$ can be made to ensure deterministic particle dynamics. Using the optimal drift (3.7) the process (3.14) becomes:

$$(3.20) \quad \frac{\text{d}}{\text{d}\tau} \mathbf{x}_\tau^{[e]} = -\mathcal{A}_\tau \nabla_{\mathbf{x}} \log \frac{q_\tau(\mathbf{x}_\tau^{[e]})}{\mathcal{P}^a(\mathbf{x}_\tau^{[e]})}, \quad \mathbf{x}_0^{[e]} = \mathbf{x}^b{}^{[e]}, \quad e = 1, \dots, \text{N}_{\text{ens}}.$$

Our numerical experience indicates that, during the first data assimilation cycles, the deterministic VFP method (3.20) works well to transform particles from background samples into analysis samples. However, after multiple assimilation cycles, the performance of the filter deteriorates considerably. Over an entire assimilation window, experiments show that a stochastic dynamics with non-zero $\boldsymbol{\sigma}(\tau, \mathbf{x})$ typically converges faster to the analysis, and yields better analysis error statistics than the deterministic dynamics.

The degradation in performance of the deterministic dynamics VFP filter is due to particles becoming “alike” through multiple forecast and assimilation cycles. This is similar to the phenomenon that causes particle collapse in particle filters, or filter divergence in EnKF. Using stochastic dynamics, i.e., a non-zero diffusion $\boldsymbol{\sigma}(\tau, \mathbf{x})$, is akin to performing rejuvenation in particle filters [2, 41], and presents a natural approach to alleviate the problem of VFP filter divergence.

Since particles are physical model states, the choice of the diffusion term should ensure that the stochastic perturbations $\boldsymbol{\sigma}(\tau, \mathbf{x})d\mathbf{W}_\tau$ do not push the particle states outside physical regimes. These perturbations should respect the scaling of different components, correlations between variables, and the quasi-equilibria of the system. To this end, a reasonable choice is to use a scaled square root of either the current particle covariance ($\boldsymbol{\sigma}(\tau) = \alpha\sqrt{2}\mathbf{Cov}[q_\tau]^{1/2}$) [18], or of a climatological covariance ($\boldsymbol{\sigma} = \sqrt{2}\alpha\mathbf{B}^{1/2}$), where α is a scaling parameter. For both these choices the diffusion is independent of the state and therefore $\mathbf{d} = 0$, simplifying the drift computation. An approximation to the square root covariance is given by the scaled ensemble anomalies ($\boldsymbol{\sigma} = \alpha\sqrt{2}(\mathbf{N}_{\text{ens}} - 1)^{-1/2}(\mathbf{X}_\tau - \bar{\mathbf{x}}_\tau)$), in which case the stochastic perturbations are similar to the rejuvenation done in ETPF [37].

3.5. Regularization of the particle flow. With a finite number of particles in a large state space particle and ensemble filters may suffer from ensemble collapse; we discussed in Subsection 3.4 that the stochastic diffusion in VFP acts as a particle rejuvenation in traditional particle filters, and alleviates the collapse. Regularization of the particle flow adds an additional drift term to the dynamics (3.1) that seeks to keep the particles spread in state space and avoid collapse. The total drift then has one component that pushes the particles toward a sample of the posterior, by minimizing the KL divergence (3.4), and a regularization component that pushes the particles apart.

3.5.1. General considerations. Before we present the motivation, we briefly discuss about exchangeable random variable, a concept useful for the motivation. A sequence of random variables whose joint distribution is invariant under any reordering is called exchangeable [38]. The concept is weaker than i.i.d (independent and identically distributed) as all i.i.d sequences are trivially exchangeable, while the vice versa is not true.

Similar to [47], we treat the ensemble $\mathbf{X}_\tau \in \mathbb{R}^{\mathbf{N}_{\text{state}} \times \mathbf{N}_{\text{ens}}}$ as a single high dimensional system of interacting particles. The ensemble is vectorized as:

$$(3.21) \quad \tilde{\mathbf{x}}_\tau = \left[\mathbf{x}_\tau^{[1]\text{T}}, \mathbf{x}_\tau^{[2]\text{T}}, \dots, \mathbf{x}_\tau^{[\mathbf{N}_{\text{ens}}]\text{T}} \right]^\text{T} \in \mathbb{R}^{\mathbf{N}_{\text{ens}}\mathbf{N}_{\text{state}} \times 1}.$$

When using a finite number of particles we have seen in subsection 3.2 and subsection 3.3 that the optimal drift term depends on the entire ensemble as we build parametric approximations of \mathcal{P}^a and q_τ ; similarly, we have seen in subsection 3.4 that the diffusion term also depends on the entire ensemble, e.g., by using the square root of the current covariance. With some abuse of notation let \mathcal{P}^a , q_τ also denote

the reconstructed probabilities, where their dependency on the ensembles is made explicit, and using (3.16) the optimal drift for each individual particle (3.15) reads:

$$(3.22a) \quad \begin{aligned} \mathbf{F}(\tau, \mathbf{x}, \mathfrak{X}_\tau) &= \mathcal{A}_\tau(\mathfrak{X}_\tau) \nabla_{\mathbf{x}} \log \mathcal{P}^a(\mathbf{x}, \mathfrak{X}^b) \\ &+ (\mathbf{D}(\tau, \mathbf{x}, \mathfrak{X}_\tau) - \mathcal{A}_\tau(\mathfrak{X}_\tau)) \nabla_{\mathbf{x}} \log q_\tau(\mathbf{x}, \mathfrak{X}_\tau) + \mathbf{d}(\tau, \mathbf{x}, \mathfrak{X}_\tau), \end{aligned}$$

and the Itô process (3.14) defines a dynamical system for all particles, coupled in the large state space $\mathbb{R}^{N_{\text{ens}} N_{\text{state}}}$ (3.21):

$$(3.22b) \quad d\mathbf{x}_\tau^{[e]} = \mathbf{F}(\tau, \mathbf{x}_\tau^{[e]}, \mathfrak{X}_\tau) d\tau + \boldsymbol{\sigma}(\tau, \mathbf{x}_\tau^{[e]}, \mathfrak{X}_\tau) d\mathbf{W}_\tau, \quad e = 1, \dots, N_{\text{ens}}.$$

Let $\mathfrak{Q}_\tau(\mathfrak{X})$ be the joint probability density of \mathfrak{X}_τ (3.21) on $\mathbb{R}^{N_{\text{ens}} N_{\text{state}}}$. Assume that a renumbering of the particles does not change the reconstructed probability densities. Specifically, if \mathfrak{X}^\dagger is the vector (3.21) assembled from particles in a different order, we have $\boldsymbol{\sigma}(\tau, \mathbf{x}, \mathfrak{X}^\dagger) = \boldsymbol{\sigma}(\tau, \mathbf{x}, \mathfrak{X})$, $q_\tau(\mathbf{x}, \mathfrak{X}^\dagger) = q_\tau(\mathbf{x}, \mathfrak{X})$, $\mathcal{A}_\tau(\mathfrak{X}^\dagger) = \mathcal{A}_\tau(\mathfrak{X})$, and $\mathcal{P}^a(\mathbf{x}, \mathfrak{X}^{b\dagger}) = \mathcal{P}^a(\mathbf{x}, \mathfrak{X}^b)$. Reordering the particles in (3.22) does not change the dynamics (except for a renumbering of particles). Consequently, the joint probability distribution $\mathfrak{Q}_\tau(\mathfrak{X})$ remains unchanged, and hence, the particles $\mathbf{x}_\tau^{[e]}$ advanced by (3.22b) are exchangeable random variables at any synthetic time τ . Consequently, the marginal probability densities of all particles are equal to each other: $q_\tau(\mathbf{x}^{[i]}) = q_\tau(\mathbf{x}^{[j]})$ for all $i, j = 1, \dots, N_{\text{ens}}$. Define the coupling term be:

$$(3.23) \quad r_\tau(\mathfrak{X}) := \mathfrak{Q}_\tau(\mathfrak{X}) / \prod_{e=1}^{N_{\text{ens}}} q_\tau(\mathbf{x}^{[e]}).$$

We now compute the optimal drift (3.7) for the coupled system of particles dynamics (3.22). The goal is to push particles toward i.i.d. samples from the posterior, therefore target probability density on $\mathbb{R}^{N_{\text{ens}} N_{\text{state}}}$ is $\mathcal{P}(\mathfrak{X}) = \prod_{e=1}^{N_{\text{ens}}} \mathcal{P}^a(\mathbf{x}^{[e]})$. Extending the formula (3.7), the e -th component of the optimal drift for the coupled set of particles is:

$$(3.24) \quad \begin{aligned} \widehat{\mathbf{F}}(\tau, \mathbf{x}_\tau^{[e]}, \mathfrak{X}_\tau) &= \mathcal{A}_\tau \nabla_{\mathbf{x}_\tau^{[e]}} \sum_{j=1}^{N_{\text{ens}}} \log \mathcal{P}^a(\mathbf{x}_\tau^{[j]}, \mathfrak{X}^b) \\ &+ (\mathbf{D}(\tau, \mathbf{x}_\tau^{[e]}) - \mathcal{A}_\tau) \nabla_{\mathbf{x}_\tau^{[e]}} \left(\sum_{j=1}^{N_{\text{ens}}} \log q_\tau(\mathbf{x}_\tau^{[j]}, \mathfrak{X}_\tau) + \log r_\tau(\mathfrak{X}_\tau) \right) + \mathbf{d}(\tau, \mathbf{x}_\tau^{[e]}, \mathfrak{X}_\tau) \\ &= \mathbf{F}(\tau, \mathbf{x}_\tau^{[e]}, \mathfrak{X}_\tau) + (\mathbf{D}(\tau, \mathbf{x}_\tau^{[e]}) - \mathcal{A}_\tau) \left(\sum_{j=1}^{N_{\text{ens}}} [\nabla_{\mathfrak{X}_\tau} \log q_\tau(\mathbf{x}_\tau^{[j]}, \mathfrak{X}_\tau)]_e + \nabla_{\mathbf{x}_\tau^{[e]}} \log r_\tau(\mathfrak{X}_\tau) \right). \end{aligned}$$

The optimal drift for the system of particles (3.24) acts on each particle e with a force equal to the optimal drift for an individual particle (3.22), plus an additional term that “corrects” for the finite number of particles. This additional term contains the gradient-log $\nabla_{\mathbf{x}_\tau^{[e]}} \log r_\tau(\mathfrak{X}_\tau)$ of the probability coupling term (3.23), plus the component of the gradient of the specific distribution parametrization $\nabla_{\mathfrak{X}_\tau} \log q_\tau(\mathbf{x}_\tau^{[j]}, \mathfrak{X}_\tau)$. This additional forcing nudges the particles toward becoming independent samples.

EXAMPLE 1. Consider the case of a multivariate Gaussian probability density:

$$(3.25) \quad \mathfrak{Q}_\tau(\mathfrak{x}) = \mathcal{N} \left(\mathfrak{x}; \begin{bmatrix} \bar{\mathbf{x}}_\tau \\ \vdots \\ \bar{\mathbf{x}}_\tau \end{bmatrix}, \begin{bmatrix} \mathbf{P}_\tau & \cdots & \hat{\mathbf{P}}_\tau \\ \vdots & \ddots & \vdots \\ \hat{\mathbf{P}}_\tau & \cdots & \mathbf{P}_\tau \end{bmatrix} \right).$$

All particle means $\bar{\mathbf{x}}_\tau$, covariances \mathbf{P}_τ , and cross-covariances $\hat{\mathbf{P}}_\tau$ are equal due to exchangeability. Marginalizing (3.25) leads to the density of each particle:

$$q_\tau(\mathbf{x}) = \mathcal{N}(\mathbf{x}; \bar{\mathbf{x}}_\tau, \mathbf{P}_\tau).$$

The negative gradient of the corresponding coupling term (3.23) reads:

$$(3.26) \quad r_\tau(\mathfrak{x}) \propto \exp \left(-\frac{1}{2} \left(\sum_{e=1}^{N_{\text{ens}}} \sum_{\substack{i=1 \\ i \neq e}}^{N_{\text{ens}}} (\mathbf{x}_\tau^{[e]} - \bar{\mathbf{x}}_\tau)^T \hat{\mathbf{P}}_\tau (\mathbf{x}_\tau^{[i]} - \bar{\mathbf{x}}_\tau) \right) \right),$$

$$-\nabla_{\mathbf{x}_\tau^{[e]}} \log r_\tau(\mathfrak{x}_\tau) = \hat{\mathbf{P}}_\tau (\mathbf{x}_\tau^{[e]} - \bar{\mathbf{x}}_\tau),$$

which is a force that pushes the particle away from the ensemble mean, therefore favoring the ensemble spread. If the particles are independent, i.e., $\hat{\mathbf{P}}_\tau = 0$ in (3.25), then this force is zero.

The drift term (3.24) that corrects for a finite number of particles and maintains the ensemble spread is difficult to estimate. For this reason we will use a regularization approach, discussed below, that acts to push the particles away from each other and favors particle independence.

3.5.2. Regularization based on mutual information. We consider a regularization term based on the mutual information between pairs of particles. The smaller the mutual information is, the closer the particles are to being independent random variables.

To be specific, consider two distinct particles with joint probability $\mathfrak{Q}_\tau(\cdot, \cdot)$, marginals $q_\tau(\cdot)$, coupling term $r_\tau(\cdot, \cdot)$ (3.23), and define $\kappa_\tau := -r_\tau \log r_\tau$. The mutual information [11] between the two distinct particles (random variables) is given by

$$I_\tau = - \int_{\Omega} \int_{\Omega} \mathfrak{Q}_\tau(\mathbf{x}, \hat{\mathbf{x}}) \log \left(\frac{\mathfrak{Q}_\tau(\mathbf{x}, \hat{\mathbf{x}})}{q_\tau(\mathbf{x})q_\tau(\hat{\mathbf{x}})} \right) d\mathbf{x} d\hat{\mathbf{x}} = \int_{\Omega} q_\tau(\mathbf{x}) \mathbb{E}_{\hat{\mathbf{x}} \sim q_\tau} [\kappa_\tau(\mathbf{x}, \hat{\mathbf{x}})] d\mathbf{x}.$$

The VFP goal is to move the particles closer to independent samples from $\mathcal{P}^a(\mathbf{x})$. In subsection 3.1 we derived the particle dynamics that minimizes $D_{\text{KL}}(q_\tau \| \mathcal{P}^a)$, the KL divergence (3.4) between the current probability density $q_\tau(\mathbf{x})$ and the posterior $\mathcal{P}^a(\mathbf{x})$. The resulting optimal drift (3.7) pushes the particles toward sampling $\mathcal{P}^a(\mathbf{x})$, but without taking into consideration the goal of particles being independent.

In order to alleviate the tendency toward particle collapse, we modify the KL divergence functional by adding a regularization term that represents the mutual information between two particles:

$$(3.27) \quad \hat{D}_{\text{KL}}(q_\tau \| \mathcal{P}^a) = D_{\text{KL}}(q_\tau \| \mathcal{P}^a) + \beta I_\tau,$$

where the parameter β determines the strength of the regularization term. Minimizing (3.27) decreases the KL divergence between the current probability density q_τ and the

posterior, but also seeks to decrease the mutual information between two particles, i.e., tends to make particles more independent.

We now derive a generalized optimal drift for the regularized cost functional (3.27).

THEOREM 3.2 (Optimal drift for the regularized cost). *The optimal drift $\widehat{\mathbf{F}}$ that minimizes the KL divergence regularized by the mutual information between two particles (3.27) is given by*

$$(3.28) \quad \widehat{\mathbf{F}}(\tau, \mathbf{x}) = \mathbf{F}(\tau, \mathbf{x}) - \beta \mathcal{A}_\tau \mathbb{E}_{\hat{\mathbf{x}} \sim q_\tau} [\nabla_{\mathbf{x}} \kappa_\tau(\mathbf{x}, \hat{\mathbf{x}})].$$

Proof. The regularized KL divergence (3.27) is written as,

$$\widehat{D}_{\text{KL}} = \int_{\Omega} q_\tau(\mathbf{x}) \left(\log \frac{q_\tau(\mathbf{x})}{p^a(\mathbf{x})} + \beta \mathbb{E}_{\hat{\mathbf{x}} \sim q_\tau} [\kappa_\tau(\mathbf{x}, \hat{\mathbf{x}})] \right) d\mathbf{x}.$$

Following the same steps as in [Theorem 3.1](#) one obtains formula (3.28) for the regularized drift $\widehat{\mathbf{F}}(\tau, \mathbf{x})$. \square

Discretizing formula (3.28) using N_{ens} particles leads to the following drift acting on each particle $e = 1, \dots, N_{\text{ens}}$:

$$(3.29) \quad \widehat{\mathbf{F}}(\tau, \mathbf{x}_\tau^{[e]}, \mathfrak{X}_\tau) = \mathbf{F}(\tau, \mathbf{x}_\tau^{[e]}, \mathfrak{X}_\tau) - \frac{\beta}{N_{\text{ens}}} \mathcal{A}_\tau \sum_{\substack{i=1 \\ i \neq e}}^{N_{\text{ens}}} \nabla_{\mathbf{x}_\tau^{[e]}} \kappa_\tau(\mathbf{x}_\tau^{[e]}, \mathbf{x}_\tau^{[i]}).$$

REMARK 5. *The function $\kappa(\mathbf{x}, \hat{\mathbf{x}})$ can be viewed as a regularization potential between a pair of states. The negative gradient $-\nabla_{\mathbf{x}_\tau^{[e]}} \kappa(\mathbf{x}_\tau^{[e]}, \mathbf{x}_\tau^{[i]})$ in (3.29) can be viewed as the corresponding repelling regularization force between particle e and another particle i ; we do not include a repelling force of a particle on itself. This also holds true in the Gaussian case, as seen in (3.26).*

Since we do not know the joint probability density $\Omega_\tau(\mathbf{x}^{[e]}, \mathbf{x}^{[i]})$ of two particles, we know neither the coupling term r_τ (3.23), nor $\kappa_\tau = r_\tau \log r_\tau$. We have two options.

- The first is to build a parametric approximation of the joint particle density $\Omega_\tau(\mathbf{x}, \hat{\mathbf{x}}, \mathfrak{X}_\tau)$ using pairs of particles as data, and use it together with the parametric approximation of the marginal $q_\tau(\mathbf{x}, \mathfrak{X}_\tau)$ to compute $\nabla_{\mathbf{x}} \kappa_\tau = -\nabla_{\mathbf{x}} r_\tau (1 + \log r_\tau)$.
- The second option is to use heuristic formulas for the regularization potential κ . For example, in this paper we choose the Coulomb potential, and the corresponding repulsive electrostatic forces:

$$(3.30) \quad \kappa(\mathbf{x}_\tau^{[e]}, \mathbf{x}_\tau^{[i]}) = \frac{1}{\|\mathbf{x}_\tau^{[e]} - \mathbf{x}_\tau^{[i]}\|_2}, \quad \nabla_{\mathbf{x}_\tau^{[e]}} \kappa(\mathbf{x}_\tau^{[e]}, \mathbf{x}_\tau^{[i]}) = -\frac{\mathbf{x}_\tau^{[e]} - \mathbf{x}_\tau^{[i]}}{\|\mathbf{x}_\tau^{[e]} - \mathbf{x}_\tau^{[i]}\|_2^3}.$$

3.6. Numerical time integration of particle dynamics. We now consider the numerical integration of the system (3.22), which is challenging due to stiffness and the presence of stochastic forcing [47]. We write the interactive particle dynamics (3.22) as

$$(3.31) \quad \begin{aligned} d\mathfrak{X}_\tau &= \mathfrak{F}(\tau, \mathfrak{X}_\tau) d\tau + \mathfrak{G}(\tau, \mathfrak{X}_\tau) d\mathfrak{W}_\tau, \\ \mathfrak{F}(\tau, \mathfrak{X}_\tau) &:= [\widehat{\mathbf{F}}(\tau, \mathbf{x}_\tau^{[1]}, \mathfrak{X}_\tau)^T, \dots, \widehat{\mathbf{F}}(\tau, \mathbf{x}_\tau^{[N_{\text{ens}}]}, \mathfrak{X}_\tau)^T]^T, \\ \mathfrak{G}(\tau, \mathfrak{X}_\tau) &:= \text{blkdiag}_{e=1 \dots N_{\text{ens}}} \{ \boldsymbol{\sigma}(\tau, \mathbf{x}_\tau^{[e]}, \mathfrak{X}_\tau) \}, \end{aligned}$$

where the drift term $\mathfrak{F} : \mathbb{R}_+ \times \mathbb{R}^{N_{\text{state}}N_{\text{ens}}} \rightarrow \mathbb{R}^{N_{\text{state}}N_{\text{ens}}}$ consists of the optimal regularized drifts for each particle (3.29), the diffusion term $\mathfrak{S} : \mathbb{R}_+ \times \mathbb{R}^{N_{\text{state}}N_{\text{ens}}} \rightarrow \mathbb{R}^{N_{\text{state}}N_{\text{ens}} \times MN_{\text{ens}}}$ is a block diagonal matrix with the diffusion terms for each particle on the diagonal, and $\mathfrak{W}\tau \in \mathbb{R}^{MN_{\text{ens}}}$ is a Wiener process.

In [47] the authors concluded that solving the interacting particle dynamics (3.31) requires infeasibly small time steps when an explicit time-stepping method is used, due to stiffness, and that further research in numerical integration is needed. Here we propose an implicit-explicit (IMEX) partitioning of the dynamics. We choose the drift to be the stiff component, and the diffusion to be the non-stiff component. We apply an IMEX numerical integration where stiff dynamics are solved implicitly and the non-stiff dynamics are solved explicitly. We note that an IMEX approach was also considered in [18] to solve the particular case of Langevin dynamics.

Since we are interested in converging to steady state, time accuracy of the integration is not important, and a low order scheme suffices. We restrict ourselves to considering linearly implicit methods that require one Jacobian calculation and one linear solve per step. Specifically, we solve the fast partition with the Rosenbrock-Euler method and the slow partition with the Euler-Maruyama method. Particle states are advanced in synthetic time from τ to $\tau + \Delta\tau$ as follows:

$$(3.32) \quad \begin{aligned} \mathfrak{X}_{\tau+\Delta\tau} = & \mathfrak{X}_{\tau} + \Delta\tau \left(\mathbf{I}_{N_{\text{state}}N_{\text{ens}}} - \Delta\tau \nabla_{\mathfrak{X}} \mathfrak{F}(\tau, \mathfrak{X}_{\tau}) \right)^{-1} \mathfrak{F}(\tau, \mathfrak{X}_{\tau}) \\ & + \sqrt{\Delta\tau} \mathfrak{S}(\tau, \mathfrak{X}_{\tau}) \boldsymbol{\xi}_{\tau}, \end{aligned}$$

where $\boldsymbol{\xi}_{\tau} \sim \mathcal{N}(\mathbf{0}, \mathbf{I}_{MN_{\text{ens}}})$. The next result from [23] shows that the proposed SDE integration method, the Rosenbrock-Euler Maruyama scheme (3.32) has the same order properties as the Euler-Maruyama.

THEOREM 3.3. *The Rosenbrock-Euler-Maruyama discretization (3.32) for time SDEs has strong order $\mathcal{O}(\Delta\tau^{\frac{1}{2}})$.*

The analytical computation of the Jacobian $\nabla_{\mathfrak{X}} \mathfrak{F}$ is complex, since each component of the function $[\mathfrak{F}]_e = \widehat{\mathbf{F}}(\tau, \mathbf{x}_{\tau}^{[e]}, \mathfrak{X}_{\tau})$ depends on all particles via the parameterizations of the underlying probability densities. It is reasonable to approximate the Jacobian by a block diagonal matrix with:

$$(3.33) \quad \nabla_{\mathfrak{X}} \mathfrak{F}(\tau, \mathfrak{X}_{\tau}) \approx \text{blkdiag}_{e=1 \dots N_{\text{ens}}} \left\{ \nabla_{\mathbf{x}} \widehat{\mathbf{F}}(\tau, \mathbf{x}, \mathfrak{X}_{\tau}) \Big|_{\mathbf{x}=\mathbf{x}_{\tau}^{[e]}} \right\},$$

which means that a linearly implicit integration is carried out for each particle separately. Assuming the diffusion terms are non-stiff we leave out their derivatives from the approximate Jacobian. From (3.7), (3.29), we have the approximation

$$\begin{aligned} \nabla_{\mathbf{x}} \widehat{\mathbf{F}}(\tau, \mathbf{x}, \mathfrak{X}_{\tau}) \Big|_{\mathbf{x}=\mathbf{x}_{\tau}^{[e]}} \approx & \mathcal{A}_{\tau} \nabla_{\mathbf{x}, \mathbf{x}}^2 \log \mathcal{P}^a(\mathbf{x}_{\tau}^{[e]}) + (\mathbf{D}(\tau, \mathbf{x}_{\tau}^{[e]}) - \mathcal{A}_{\tau}) \nabla_{\mathbf{x}, \mathbf{x}}^2 \log q_{\tau}(\mathbf{x}_{\tau}^{[e]}) \\ & - \frac{\beta}{N_{\text{ens}}} \mathcal{A}_{\tau} \sum_{i \neq e} \nabla_{\mathbf{x}, \mathbf{x}}^2 \kappa_{\tau}(\mathbf{x}, \mathbf{x}_{\tau}^{[i]}) \Big|_{\mathbf{x}=\mathbf{x}_{\tau}^{[e]}}. \end{aligned}$$

To avoid these calculations, in this paper we use a finite difference approximation of Jacobian-vector products, and solve the linear system (3.32) using GMRES [49]. We refer the reader to [54] for more details. This is not only less expensive, but potentially captures the parametric interactions not captured by the analytical derivatives above. These methods can however be impractical for large systems, and thus, the numerical solution of particle dynamics remains an open problem.

REMARK 6. The time-stepping problem (3.31) can be seen as an optimization problem with $\mathfrak{F}(\tau, \mathfrak{X}_\tau)$ the negative gradient of the cost function. Methods for performing large scale deterministic optimization such as ADAM [27] can also be used as alternatives to the scheme provided herein.

REMARK 7. Under the limit of ensemble size, $N_{\text{ens}} \rightarrow \infty$, the expected value or the mean of the dynamics will be deterministic, thus, giving us a condition for early termination of the time evolution. The time evolution is stopped at some finite time τ_* when the change in the statistical mean $\bar{\mathbf{x}}_\tau$ of the particles \mathbf{X}_τ is under a chosen tolerance threshold ϵ , indicating that steady state was achieved:

$$(3.34) \quad \|\bar{\mathbf{x}}_{\tau_* + \Delta\tau} - \bar{\mathbf{x}}_{\tau_*}\| < \epsilon \Delta\tau.$$

4. Examples of particular VFP filters and smoothers. As noted in Subsection 3.2, the drift term (3.15) approximation in the VFP can be completely described by the choice of parameterization of the prior and intermediate distributions, along with the distribution of the observation errors (assumed to be known). We discuss several examples of choices of parametric distributions.

4.1. Gaussian assumptions. We first discuss the case of unbiased Gaussian errors (see Table 3.1). The background error probability density is assumed to be $\mathcal{P}^b(\mathbf{x}) = \mathcal{N}(\mathbf{x} | \bar{\mathbf{x}}^b, \mathbf{P}^b)$. The intermediate probability densities are assumed Gaussian, $q_\tau(\mathbf{x}) = \mathcal{N}(\mathbf{x} | \bar{\mathbf{x}}_\tau, \mathbf{P}_\tau)$.

The known observation likelihood is assumed to be $\mathcal{P}^{\text{obs}}(\mathbf{x}) = \mathcal{N}(\mathbf{x} | \mathcal{H}(\mathbf{x}) - \mathbf{y}, \mathbf{R})$, where \mathbf{y} is the observation value (2.1), \mathbf{R} is the observation error covariance, and \mathcal{H} is the observation operator.

By (3.16) and under Gaussian assumptions on the prior, intermediate, and observation distributions, the optimal drift (3.11) is:

$$(4.1) \quad \begin{aligned} \mathbf{F}(\tau, \mathbf{x}_\tau) = & -(\mathbf{P}^b)^{-1}(\mathbf{x}_\tau - \bar{\mathbf{x}}^b) - \mathbf{H}^T \mathbf{R}^{-1}(\mathcal{H}(\mathbf{x}_\tau) - \mathbf{y}) \\ & - (\mathbf{D}(\tau, \mathbf{x}_\tau) - \mathbf{I}_{N_{\text{state}}})(\mathbf{P}_\tau)^{-1}(\mathbf{x}_\tau - \bar{\mathbf{x}}_\tau) + \mathbf{d}(\tau, \mathbf{x}_\tau). \end{aligned}$$

\mathbf{H}^T is the adjoint of \mathcal{H} . As discussed in Subsection 3.2, this approach is termed VFP(GG) to denote the Gaussian assumptions on the prior and intermediate distributions respectively.

For Gaussian assumptions on both the prior and intermediate distributions, and Cauchy observation errors (see Table 3.1), the optimal drift (3.11) in the VFP(GG) approach is now,

$$(4.2) \quad \begin{aligned} \mathbf{F}(\tau, \mathbf{x}_\tau) = & -(\mathbf{P}^b)^{-1}(\mathbf{x}_\tau - \bar{\mathbf{x}}^b) - \frac{N_{\text{state}} + 1}{1 + \|\mathcal{H}(\mathbf{x}_\tau) - \mathbf{y}\|_{\mathbf{R}^{-1}}^2} \mathbf{H}^T \mathbf{R}^{-1}(\mathcal{H}(\mathbf{x}) - \mathbf{y}), \\ & - (\mathbf{D}(\tau, \mathbf{x}_\tau) - \mathbf{I}_{N_{\text{state}}})(\mathbf{P}_\tau)^{-1}(\mathbf{x}_\tau - \bar{\mathbf{x}}_\tau) + \mathbf{d}(\tau, \mathbf{x}_\tau), \end{aligned}$$

where \mathbf{R} is a measure of scale in the Cauchy distribution.

4.2. Laplace prior error assumptions. We now consider the example of the VFP filter under Laplace assumptions on the prior \mathcal{P}^b and Gaussian assumptions on the intermediate distributions q_τ (see Table 3.1), which we name the VFP(LG). For a Gaussian observation likelihood \mathcal{P}^{obs} , the optimal drift term (3.15) is:

$$(4.3) \quad \begin{aligned} \mathbf{F}(\tau, \mathbf{x}_\tau) = & -\frac{2}{\theta^b} \frac{\mathcal{K}_{\nu-1}(\theta^b)}{\mathcal{K}_\nu(\theta^b)} (\mathbf{P}^b)^{-1}(\mathbf{x}_\tau - \bar{\mathbf{x}}^b) - \mathbf{H}^T \mathbf{R}^{-1}(\mathcal{H}(\mathbf{x}_\tau) - \mathbf{y}) \\ & - (\mathbf{D}(\tau, \mathbf{x}_\tau) - \mathbf{I}_{N_{\text{state}}})(\mathbf{P}_\tau)^{-1}(\mathbf{x}_\tau - \bar{\mathbf{x}}_\tau) + \mathbf{d}(\tau, \mathbf{x}_\tau), \end{aligned}$$

where $\theta^b = \sqrt{2} \|\mathbf{x} - \bar{\mathbf{x}}^b\|_{(\mathbf{P}^b)^{-1}}$, $\nu = 1 - N_{\text{state}}/2$.

4.3. Variational particle smoothing. The VFP framework can also handle smoothing (2.5), where all observations in a window are assimilated at once. Following (3.18), we make a Gaussian assumption on the prior initial conditions $\mathcal{P}^b = \mathcal{N}(\mathbf{x} | \bar{\mathbf{x}}_0^b, \mathbf{P}_0^b)$, and Gaussian assumptions on the intermediate distributions, $q_\tau(\mathbf{x}) = \mathcal{N}(\mathbf{x} | \bar{\mathbf{x}}_{0,\tau}, \mathbf{P}_{0,\tau})$. The known observation likelihood at physical time t_k is assumed to be $\mathcal{P}_k^{\text{obs}}(\mathbf{x}) = \mathcal{N}(\mathbf{x} | \mathcal{H}_k(\mathbf{x}) - \mathbf{y}_k, \mathbf{R}_k)$, where \mathbf{y}_k are the observations. The optimal drift (3.15) is:

$$(4.4) \quad \mathbf{F}(\tau, \mathbf{x}_{0,\tau}) = -(\mathbf{P}_0^b)^{-1}(\mathbf{x}_{0,\tau} - \bar{\mathbf{x}}_0^b) - \sum_{k=1}^K \mathbf{H}_k^\top \mathbf{M}_{0,k}^\top \mathbf{R}_k^{-1} (\mathcal{H}_k(\mathcal{M}_{0,k}(\mathbf{x}_{0,\tau})) - \mathbf{y}_k) \\ - (\mathbf{D}(\tau, \mathbf{x}_{0,\tau}) - \mathbf{I}_{\text{N}_{\text{state}}})(\mathbf{P}_{0,\tau})^{-1}(\mathbf{x}_{0,\tau} - \bar{\mathbf{x}}_{0,\tau}) + \mathbf{d}(\tau, \mathbf{x}_{0,\tau}),$$

where $\mathbf{x}_{0,\tau}$ is one initial condition (particle), and \mathbf{M}^\top is the adjoint of the model operator (2.3). We term VFPS the VFP smoother, and name the approach in (4.4) as the VFPS(GG).

REMARK 8. *The first two terms in (4.4) are the 4D-Var gradient. The additional term $(\mathbf{P}_{0,\tau})^{-1}(\mathbf{x}_{0,\tau} - \bar{\mathbf{x}}_{0,\tau})$ pushes each particle away from the intermediate ensemble mean. VFPS with Gaussian assumptions is a regularized ensemble 4D-Var method that seeks to sample the posterior distribution. In contrast, the traditional 4D-Var approach seeks only a mode of the posterior distribution.*

5. Illustration of the VFP approach. Next, we provide several trivial numerical examples to highlight the VFP approach. In the following subsection, we demonstrate diffusion and regularization in the VFP for a 2-D problem. Then, the subsection after that describes the methodology of performing VFP assimilation with multimodal priors and observations.

5.1. Demonstration of regularization and diffusion. For the first demonstration, we look at the effects of the diffusion component in the Itô process (3.14) and the regularization component in the augmented drift (3.29), as applied to a simple ensemble.

We aim to analyze the difference between four different methods with Gaussian and Laplace assumptions on the prior and intermediate distributions (see Table 3.1). We analyze VFP(GG), VFP(GL), VFP(LG), and VFP(LL) where the first letter represents the prior assumption and the second the intermediate assumption.

Four sets of prior ensembles are taken, coupled with a simple Gaussian observation, and evolved through the ensemble Itô process (3.14).

Three experiments are performed (i) assimilation in the absence of both diffusion and regularization, (ii) assimilation in the presence of diffusion only, (iii) assimilation in the presence of regularization only. The results of these experiments can be seen in subsection 5.1, with the prior ensembles described by subsection 5.1.

Without diffusion or regularization subsection 5.1, VFP(LG) and VFP(LL) suffer from ensemble collapse in one step. The fully Gaussian VFP(GG) has a diverse set of samples both close to and far away from the mean, while VFP(GL) forms a ring around the mean.

With the addition of diffusion in subsection 5.1, all the ensembles have a diverse set of particles both close to and far from the analysis means. The ensembles of VFP(LG) and VFP(LL) no longer suffer from ensemble collapse, and the ensemble of VFP(GL) shows a much weaker ring-like structure. The ensemble of VFP(GG) does not seem to have any qualitative difference as opposed to that without diffusion.

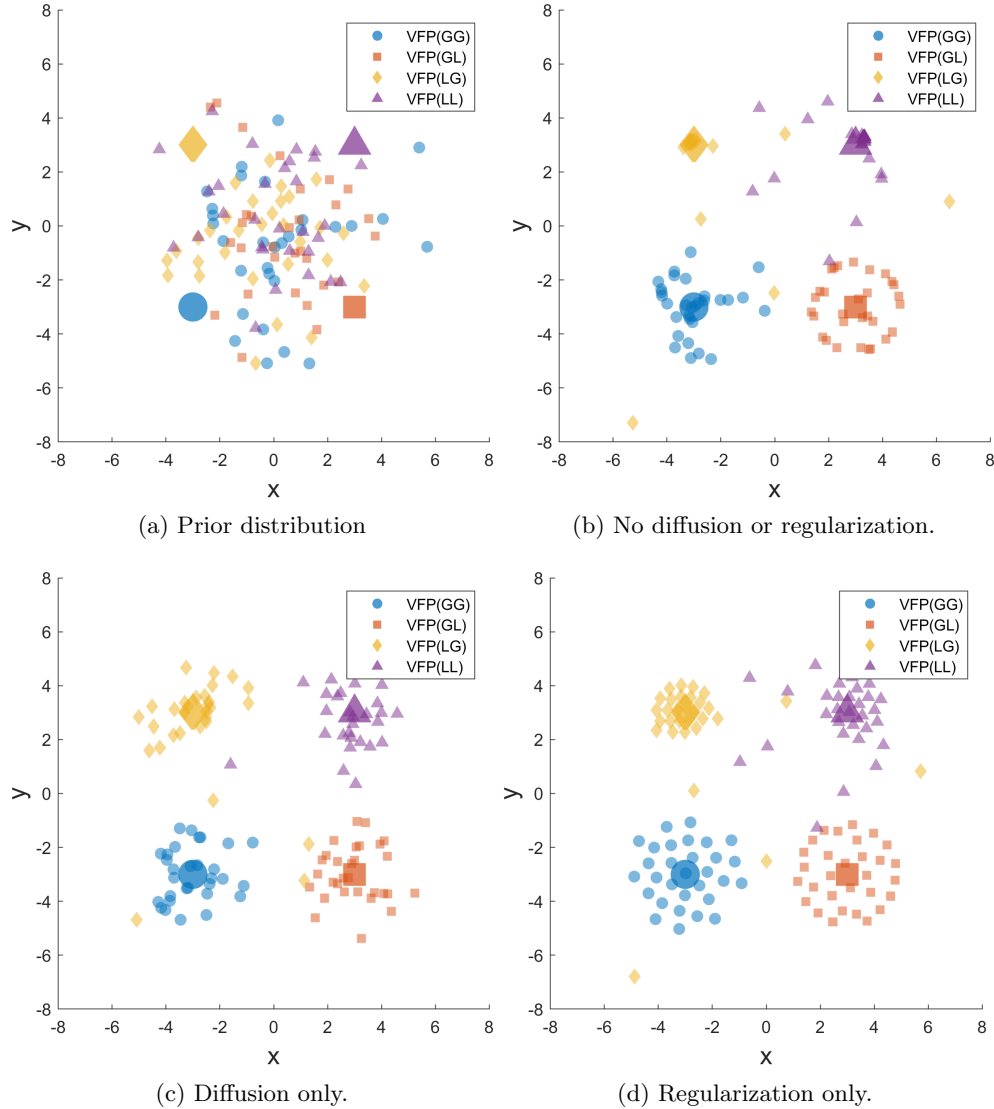


Fig. 5.1: A comparison of the analysis distributions of VFP(GG), VFP(GL), VFP(LG), and VFP(LL) based on different diffusion and regularization strategies. The four large symbols represent the means of the four posteriors and the smaller symbols represent the analysis particles.

With the addition of regularization in [subsection 5.1](#), all the particles seem to have much more uniform distribution along their support, with each method having its own unique circle-like structure. The problematic methods VFP(LG) and VFP(LL) still seem to suffer from ensemble collapse, VFP(GL) still preserves a distinct ring-like structure around the whole ensemble, and VFP(GG) seems like non-independent sampling.

From these results we are able to ascertain that both diffusion and regularization

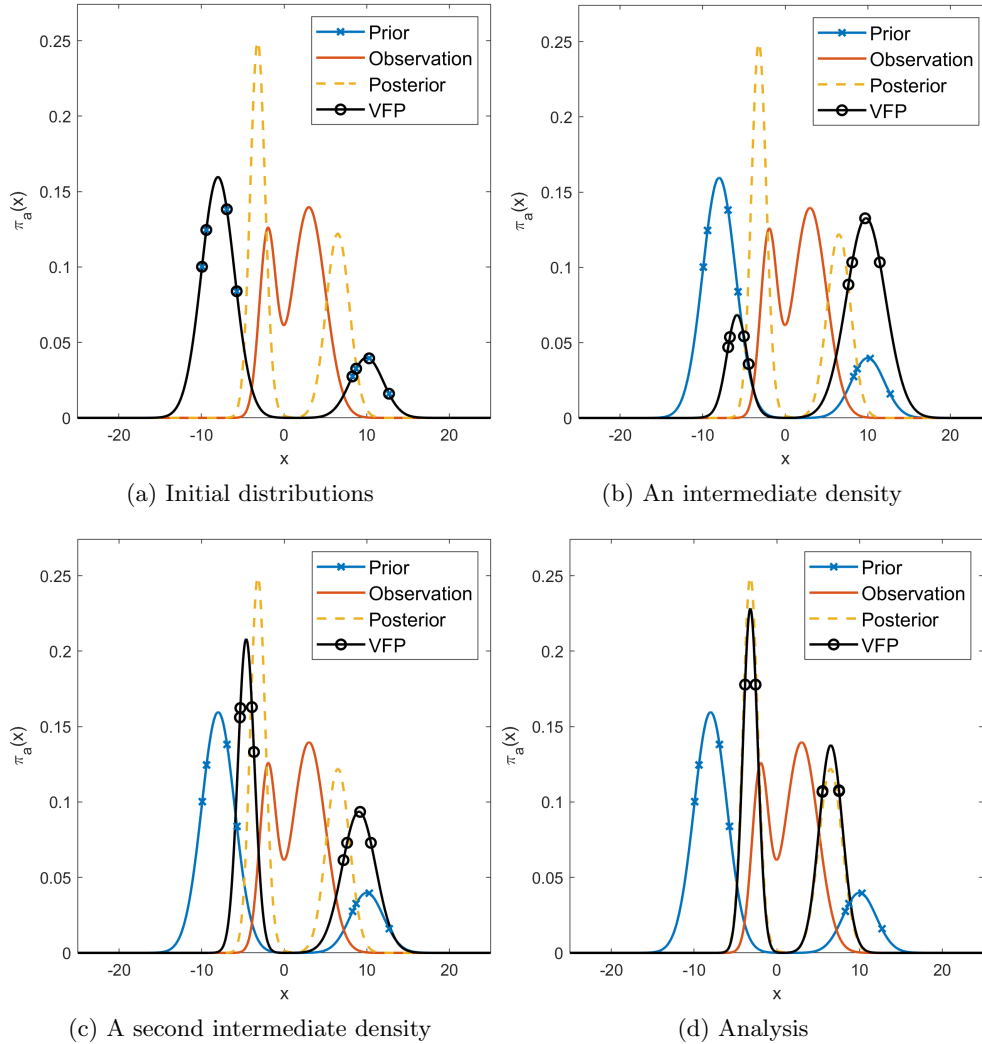


Fig. 5.2: This example compares the analysis for a Gaussian mixture. Though there are 4 modes, the 2 weak modes get subsumed by the 2 dominant modes in both the exact posterior and our analysis.

play important roles in achieving optimal ensemble-based inference.

5.2. Demonstration of multimodal assimilation. We now show on a simple one dimensional example how the VFP can be utilized for multimodal data assimilation.

Let the prior distribution have M_f modes and the observation distribution M_o modes. Then, the posterior must have at most $M_f \times M_o$ modes, which in practice is much lesser as many weaker modes get subsumed by stronger modes.

For assimilation, the prior ensemble is first clustered into its M_f sub-ensembles, each of which are further divided into M_o different sub-sub-ensembles. Each sub-

sub-ensemble performs assimilation in a parallel fashion for its respective prior and observation distributions. When all sub-sub-ensembles have completed assimilation, we have the ensemble analysis.

However, to reconstruct the optimal analysis distribution, it must be stitched together in a specific fashion. First, weights are estimated for each analysis particle to be equal to their observational likelihood,

$$(5.1) \quad \mathbf{w} = \mathcal{P}^{\text{obs}}(\mathbf{X}^a).$$

The total weight for each sub-sub-ensemble is calculated by adding the weights of all the particles within that sub-sub-ensemble,

$$(5.2) \quad \mathbf{w}_{i,j} \propto \sum \mathbf{w}, \quad i = 1, \dots, M_f, \quad j = 1, \dots, M_o,$$

with the weights for each sub-sub-ensemble normalized by their sum to have the total weight of the full ensemble equal to one.

Based on the distribution assumption, the analysis distribution is calculated as a weighted sum of every sub-sub-analysis distribution where the weights come from the aforementioned calculation in (5.2) and the distribution is assumed in a parameterized sense. Though this approach can be extended to high dimensional problems, it is an open question if this is the best approach to multimodal analysis under the VFP framework.

In subsection 5.2, we assume a bimodal Gaussian mixture prior and a bimodal observation distribution in a one-dimensional setting and perform one assimilation step using VFP(GG). Though there is a slight discrepancy between the exact posterior distribution and the constructed analysis, each of the dominant modes are accurately captured.

6. Localization and covariance shrinkage. As the prior and intermediate distributions are parameterized, certain assumptions on the distributions require the online estimation of the respective covariance matrices. In high dimensional systems, when $N_{\text{ens}} \ll N_{\text{state}}$, the estimated low-rank covariance has spurious correlations between the states. In most systems of interest, which are spatially-defined, the correlations between any two states is inversely proportional to their distance. The VFP formulation permits the usage of localization and covariance shrinkage to ameliorate the issues with covariance estimation.

6.1. Schur-product localization with local update. Schur-product localization [4,39] corrects the covariance estimate by performing an element-wise product of the covariance \mathbf{P}_τ with a decorrelation matrix \mathbf{C} that is a function of the distances between the states. Let $d(i, j)$ be a metric between the i th and j th states of the system. Then, the covariance estimate is given by,

$$(6.1) \quad (\mathbf{P}_\tau)_{\text{loc}} = \mathbf{P}_\tau \circ \mathbf{C}, \quad \text{where } \mathbf{C}_{i,j} = \rho\left(\frac{d(i, j)}{r}\right),$$

where, $\rho(\cdot)$ is a chosen decorrelation function and r is the decorrelation radius. Popular choices for the decorrelation function are the Gaussian and the piecewise rational Gaspari-Cohn [19] with compact support. The decorrelation function used in this

work is the Gaspari-Cohn given by:

$$(6.2) \quad \rho(\zeta) = \begin{cases} -\frac{1}{4} \left(\frac{\zeta}{\theta}\right)^5 + \frac{1}{2} \left(\frac{\zeta}{\theta}\right)^4 + \frac{5}{8} \left(\frac{\zeta}{\theta}\right)^3 - \frac{5}{3} \left(\frac{\zeta}{\theta}\right)^2 + 1 & 0 \leq \zeta \leq \theta, \\ \frac{1}{12} \left(\frac{\zeta}{\theta}\right)^5 - \frac{1}{2} \left(\frac{\zeta}{\theta}\right)^4 + \frac{5}{8} \left(\frac{\zeta}{\theta}\right)^3 + \frac{5}{3} \left(\frac{\zeta}{\theta}\right)^2 - 5 \left(\frac{\zeta}{\theta}\right) + 4 - \frac{2}{3} \left(\frac{\theta}{\zeta}\right) & \theta < \zeta \leq 2\theta, \\ 0 & \text{otherwise,} \end{cases}$$

with an optimally chosen parameter θ . Since the Gaspari-Cohn function has compact support, the decorrelation matrix \mathbf{C} will be sparse.

In the local-update approach, we first calculate the localized states to be used in the gradient computation for each state variable. Formally, for state i , we have the localized set of indices $\mathcal{I}_i \in \{1, \dots, N_{\text{state}}\}$, obtained as

$$(6.3) \quad \{j\} \in \mathcal{I}_i \text{ if } \rho\left(\frac{d(i,j)}{r}\right) > 0 \text{ for } j = 1, \dots, N_{\text{state}}.$$

Next, the local ensemble is written as $\mathbf{X}_{\tau,i} = \mathbf{X}_{\tau}(\mathcal{I}_i, \cdot)$, which is used to calculate the local mean $\bar{\mathbf{x}}_{\tau,i}$, anomalies $\mathbf{A}_{\tau,i}$ and covariance $\mathbf{P}_{\tau,i}$ as (2.8). For a Gaussian assumption on the intermediate, a localized version of $\nabla_{\mathbf{x}} \log q_{\tau}$ for state i can be written as

$$(6.4) \quad \nabla_{\mathbf{x}} \log q_{\tau}(\mathbf{x}_{\tau,i}) = -(\mathbf{P}_{\tau,i})^{-1} (\mathbf{x}_{\tau,i} - \bar{\mathbf{x}}_{\tau,i}).$$

Similarly, we estimate $\sigma(\tau, \mathbf{x}_{\tau,i})$ and the other gradient terms in $\mathbf{F}(\tau, \mathbf{x}_{\tau,i})$. The Wiener process $\mathbf{W}_{\tau,i}$ is now different for each state i and potentially lives in a smaller dimension. The i th state is updated by time stepping only the i th component of $\mathbf{F}(\tau, \mathbf{x}_{\tau,i})$ and $\sigma(\tau, \mathbf{x}_{\tau,i}) \mathbf{W}_{\tau,i}$.

6.2. Covariance shrinkage. When the analysis and intermediate distributions in the drift (3.15) are assumed Gaussian Table 3.1, covariance shrinkage methods [8] can be used to correct the covariance. In this work, the Rao-Blackwell Ledoit-Wolf shrinkage estimator is specifically used. For an ensemble \mathbf{X}_{τ} , the shrinkage covariance,

$$(6.5) \quad (\mathbf{P}_{\tau})_{\text{RBLW}} = (1 - \gamma) \mathbf{P}_{\tau} + \gamma \hat{\Sigma}_{\tau}$$

$$(6.6) \quad \gamma = \min \left(\frac{\left[\frac{N_{\text{ens}} - 2}{N_{\text{ens}}} \text{trace}(\mathbf{P}_{\tau}^2) \right] + \text{trace}^2(\mathbf{P}_{\tau})}{(N_{\text{ens}} + 2) \left[\text{trace}(\mathbf{P}_{\tau}^2) - \frac{\text{trace}^2(\mathbf{P}_{\tau})}{N_{\text{state}}} \right]}, 1 \right)$$

can be utilized, where the $\mathbf{P}_{\tau} = \mathbf{A}_{\tau} \mathbf{A}_{\tau}^{\text{T}}$ is covariance of samples, and the target covariance $\hat{\mathbf{P}}_{\tau}$,

$$(6.7) \quad \hat{\Sigma}_{\tau} = \frac{\text{trace}(\mathbf{P}_{\tau})}{N_{\text{state}}} \mathbf{I}_{N_{\text{state}}} = \mu \mathbf{I}_{N_{\text{state}}},$$

is chosen to be the trace-normalized identity. For example, we can rewrite $\nabla_{\mathbf{x}} \log q_{\tau}$ with covariance shrinkage as

$$(6.8) \quad \begin{aligned} \nabla_{\mathbf{x}} \log q_{\tau}(\mathbf{x}_{\tau}) &= -(\mathbf{P}_{\tau})_{\text{RBLW}}^{-1} (\mathbf{x}_{\tau} - \bar{\mathbf{x}}_{\tau}) \\ &= -\frac{(\mathbf{x}_{\tau} - \bar{\mathbf{x}}_{\tau})}{\gamma \mu} - \frac{1 - \gamma}{(\gamma \mu)^2} \mathbf{A}_{\tau} \left(\mathbf{I}_{N_{\text{ens}}} + \frac{1 - \gamma}{\gamma \mu} \mathbf{A}_{\tau}^{\text{T}} \mathbf{A}_{\tau} \right)^{-1} \left(\mathbf{A}_{\tau}^{\text{T}} (\mathbf{x}_{\tau} - \bar{\mathbf{x}}_{\tau}) \right), \end{aligned}$$

using the Sherman-Morrison-Woodbury identity to invert $(\mathbf{P}_{\tau})_{\text{RBLW}}$.

7. Numerical experiments. We now illustrate the effectiveness of the VFP and compare it to other state-of-the-art methods with the help of several numerical experiments. One of the metrics that is traditionally used to evaluate assimilation methods is spatio-temporal RMSE. Spatio-temporal RMSE is calculated as

$$(7.1) \quad \text{RMSE} = \sqrt{\frac{1}{\text{KN}_{\text{state}}} \sum_{k=1}^K (\mathbf{x}_k^{\text{true}} - \bar{\mathbf{x}}_k^{\text{a}})^T (\mathbf{x}_k^{\text{true}} - \bar{\mathbf{x}}_k^{\text{a}})}$$

where K represents every assimilation step post spinup, and $\bar{\mathbf{x}}_k^{\text{a}}$ is the analysis mean at time t_k . All test problems and implementations are from the ODE Test problems suite [10, 48].

7.1. The Lorenz '63 test problem. For our first round of experiments, we use the canonical 3-variable Lorenz '63 model [35],

$$(7.2) \quad \frac{dx}{dt} = \sigma(y - x), \quad \frac{dy}{dt} = x(\rho - z) - y, \quad \frac{dz}{dt} = xy - \beta z,$$

to showcase various properties of our formulation. We set the parameters in (7.2) to their canonical values of $\sigma = 10$, $\rho = 28$, $\beta = 8/3$ which results in chaos.

The model is assumed to be exact, and is propagated in time using the Dormand-Prince 5(4) method [13]. The following Lorenz '63 experiments are run for 55000 steps ignoring statistics from the 5000 as spinup. Each experiment is repeated 12 times with different random seeds with the results averaged to ensure robustness. The observations are assimilated every $\Delta t = 0.12$, which is equivalent to an atmospheric time scale of 9 hours [53]. We observe all three variables with either unbiased Gaussian error with covariance $\mathbf{R} = 8\mathbf{I}_3$, or with Cauchy observation error with $\mathbf{R} = \mathbf{I}_3$. Each experiment is repeated 12 times with different random seeds with the results averaged to ensure robustness.

7.1.1. Effect of diffusion and regularization on an ensemble rank histogram. In this first experiment we wish to analyze the quality of the analysis ensemble by varying the diffusion and regularization coefficients.

Rank histograms [20] evaluate the accuracy of ensemble predictions by analyzing the error with the ensemble mean and spread. A good ensemble prediction method is one that has a uniform rank histogram. In our experiment, a rank histogram of the first variable of the analysis is constructed with the true trajectory taken as the reference.

For diffusion we use $\sigma(\mathbf{x}_\tau) = \alpha \mathbf{A}^{\text{b}}$ where \mathbf{A}^{b} are the scaled background ensemble anomalies defined by (2.8), and τ is a parameter. For regularization we use the electrostatic force (3.30) with β as the parameter.

The VFP(GG) method is used as the assimilation scheme with the noisy Gaussian unbiased error covariance of $8\mathbf{I}_3$, and an ensemble size of $N_{\text{ens}} = 50$. The parameters are varied as follows: $\tau = \{0, 0.001, 0.01, 0.1\}$ and $\beta = \{0, 0.01, 0.1, 1\}$.

Subsection 7.1.1 provided a visual overview of the results of this experiment. It is clear that for a low and high values of the regularization parameter β , the rank histogram tends away from a uniform distribution. For diffusion on the other hand, the higher the value, the more uniform the rank histogram becomes.

Based on subsection 7.1.1, we choose $\tau = 0.1$ and $\beta = 0.01$ for the subsequent experiments on the Lorenz '63 system, with the caveat that these values may be optimal only for this particular setting.

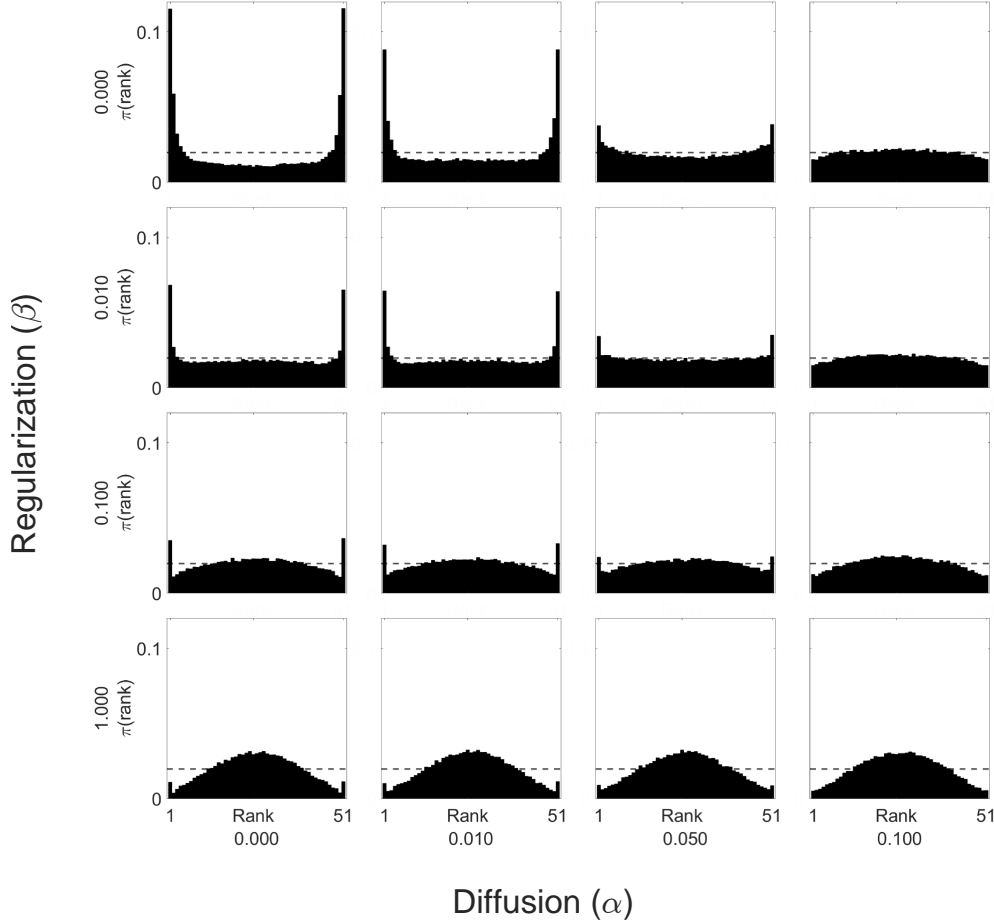


Fig. 7.1: Rank histograms for 50 particles obtained at different parameter values of the diffusion parameter α and the regularization parameter β . The ideal parameter choice is the one that gives a uniform rank histogram.

7.1.2. Gaussian observation error. We use the standard experimental setup consisting of a linear observation operator $\mathcal{H}(\mathbf{x}) = \mathbf{x}$ and unbiased Gaussian observation error covariance $R = 8\mathbf{I}_3$. We modify the ensemble size N and observe the analysis RMSE (7.1) for each one.

We present 4 different formulations of the variational Fokker-Planck, namely, the VFP(KK), VFP(GG), VFP(GH), VFP(HH), and VFPLang(G) schemes (see Table 3.1 for more details about the distributions underlying these assumptions). For the Huber distribution parameters we choose $\delta_1 = \delta_2 = 1$ based on empirical performance. The VFP(KK) scheme will serve in the place of the MPF, as they are nearly identical in form and function, with the kernel covariance parameter computed in a similar fashion to [42]. These schemes will be compared to the ETKF (with an optimal inflation for each ensemble size N_{ens}), ETPF and the second order accurate ETPF (ETPF2). For the baseline theoretical lower-bound error the sequential importance resampling particle filter (SIR) with an ensemble size of $N_{\text{ens}} = 10000$ particles is

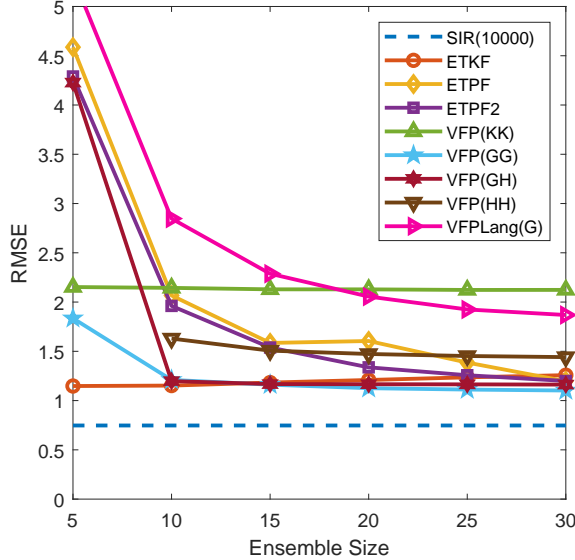


Fig. 7.2: A comparison of the RMSE of multiple VFP assumptions, ETKF, ETPF and SIR baseline, for the Lorenz-63 problem having a Gaussian observation covariance of $\mathbf{R} = 8\mathbf{I}_3$.

utilized, as in the limit $N_{\text{ens}} \rightarrow \infty$ it performs exact Bayesian inference. The analysis RMSE for this line of experiments can be seen in [subsection 7.1.2](#) for various ensemble sizes N_{ens} .

The VFP(GG) and ETKF both approximate fully-Gaussian inference and can be seen as different discretizations of the Kalman filter, thus it is not surprising that their performance is the same. The VFP(HH) shows a slightly higher RMSE, which may be due to the fact that the underlying Laplace distribution is super-Gaussian, while the support of the dynamics of the system is sub-Gaussian [58]. The VFP(KK) has poor performance, meaning that the MPF would likely also perform poorly on this problem formulation.

7.1.3. Cauchy observation error. The settings for this experiment are the same as the Lorenz '63 with Gaussian observations in [Subsection 7.1.2](#), except for the observation distribution, which is set to the Cauchy distribution with scale parameter $\mathbf{R} = \mathbf{I}_3$. The analysis RMSE for this line of experiments can be seen in [subsection 7.1.3](#) for various ensemble sizes N_{ens} .

The ETKF fails to converge for any observation covariance choice as the distribution of the observations is non-Gaussian. The VFP(HH) also fails to converge.

The VFP(KK) (and likely the MPF) performs really poorly for these given settings, likely because of poor choices for the Kernel covariances.

The VFP(GG) and VFP(GH) perform similarly well, with the VFP(GH) performing slightly better likely because of the slight super-Gaussianity of the Huber distribution being more similar to the Cauchy distribution of the observations.

Although some of the VFP methods perform better than the purely Gaussian ETKF, they still perform worse than the purely non-Gaussian ETPF family of meth-

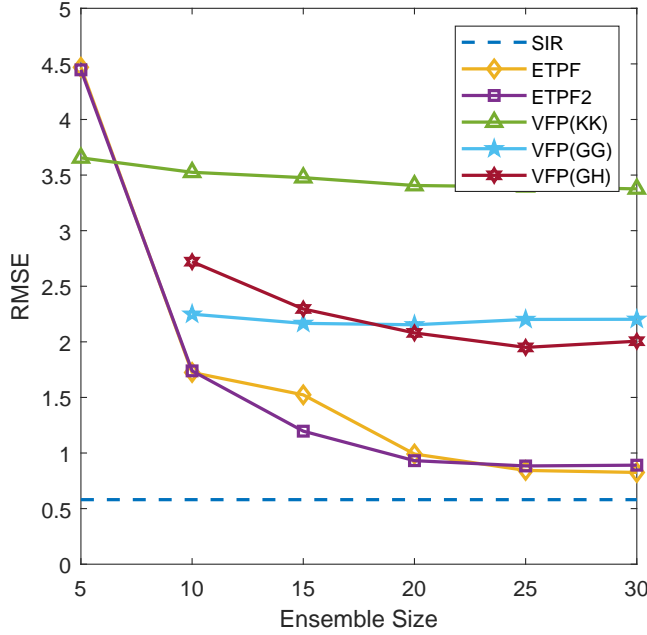


Fig. 7.3: A comparison of the RMSE of multiple VFP assumptions, ETPF and SIR baseline, for the Lorenz-63 problem having a Cauchy observation error covariance with scale $\mathbf{R} = \mathbf{I}_3$

ods. This leads us to conclude that the VFP can act as a bridge between Gaussian filtering and non-Gaussian filtering.

7.2. The Lorenz '96 test problem. The next experiment is performed on the 40-variable Lorenz '96 problem [34, 55] given by

$$(7.3) \quad \frac{dx_i}{dt} = (x_{i+1} - x_{i-2})x_{i-1} - x_i + F, \quad \text{for } i = 1, \dots, 40 \quad \text{and } F = 8,$$

where the cyclic boundary conditions $x_{-1} = x_{39}$, $x_0 = x_{40}$ and $x_{41} = x_1$ apply. This is a traditional, medium-sized problem that is chosen to mostly showcase localization for any data assimilation method.

The Dormand-Prince 5(4) [13] is used for time-stepping the dynamical system with a time span of $\Delta t = 0.05$ which corresponds to six hours in real time. We assimilate for 2200 cycles discarding the first 200. The experiment is averaged over 12 different random seeds. We observe all variables with the linear observation operator $\mathcal{H}(\mathbf{x}) = \mathbf{x}$ along with the unbiased Gaussian error covariance $\mathbf{R} = \mathbf{I}_{40}$. The diffusion and regularization are chosen as $\alpha = 1e - 1$ and $\beta = 0$.

We will look at three different localized (see Subsection 6.1) versions of the VFP filters and smoothers, a localized Gaussian prior Gaussian intermediate filter LVFP(GG), a localized Gaussian prior Kernel intermediate filter LVFP(GK), and a localized variant of (4.4) which is a Gaussian prior Gaussian intermediate smoother LVFPS(GG). While Schur-localization is performed on the LVFPS(GG), local update is not. The LVFP(GK) is a variant of the particle flow filter (PFF) introduced in [22].

We compare the VFP methods to the localized ensemble transform Kalman filter (LETKF) [24], and a localized ensemble transform Kalman smoother LETKS [5].

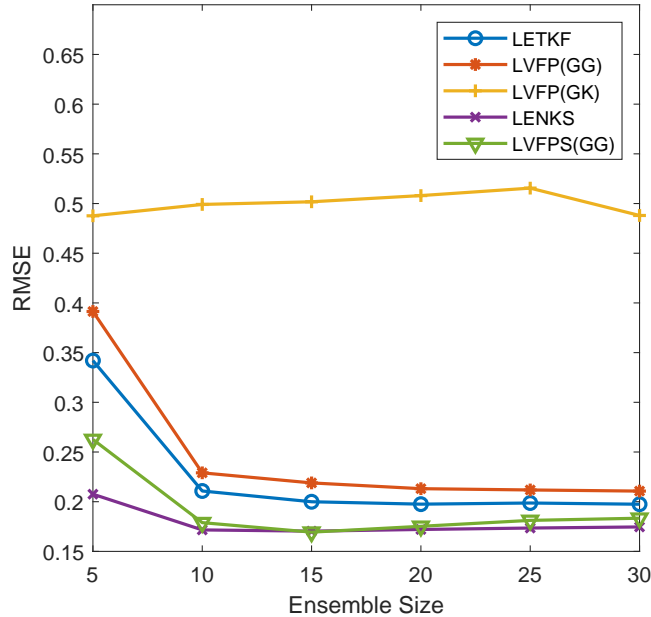


Fig. 7.4: For the Lorenz '96 equations ensemble size N_{ens} is compared to the analysis RMSE. Various localized VFP filters and a smoother are compared to the standard LETKF and LETKS.

The Gaspari-Cohn decorrelation function (6.2) with a radius of 4 units is used for all localization. For the smoothers, a look-ahead window of $K = 5$ is considered.

We compared several different ensemble sizes N_{ens} to the analysis RMSE. The results of these experiments are shown in subsection 7.2. The two Gaussian filters, the LVFP(GG) and the LETKF, have very similar performance. Likewise, the two smoothers, the LVFPS(GG) and LETKS also have similar performance. The particle flow filter LVFP(GK), however, had significantly higher errors for this problem setup.

7.3. The quasi-geostrophic equations test problem. The quasi geostrophic equations [51] approximate oceanic and atmospheric dynamics where the Coriolis and pressure gradient forces are almost balanced. The PDE can be written as:

$$(7.4) \quad \begin{aligned} \omega_t + \mathbf{J}(\psi, \omega) - Ro^{-1}\psi_x &= Re^{-1}\Delta\omega + Ro^{-1}\mathbf{F}, \\ \mathbf{J}(\psi, \omega) &\equiv \psi_y\omega_x - \psi_x\omega_y, \quad \mathbf{F} = \sin(\pi(y-1)), \quad \omega = -\Delta\psi \end{aligned}$$

where ω is the vorticity, ψ is the streamfunction, $Re = 450$ is the Reynolds number, $Ro = 0.0036$ is the Rossby number, \mathbf{J} is the non-linear Jacobian, and \mathbf{F} is the symmetric double gyre forcing term. The domain is defined to be $\Omega = [0, 1] \times [0, 2]$ which is discretized on a $63 \times 127 = 8001$ grid. The homogeneous Dirichlet boundary condition of $\psi_{\partial\Omega} = 0$ is assumed for all time. The problem represents

Our results consider the spatio-temporal RMSE for 400 steps discarding the first 50 as spinup, averaged over 12 different random seeds. Observations are assimilated every $\Delta t = 0.0109$ time units that is approximately one day in the atmospheric time scale. We observe 150 evenly spaced states between 1 and 8001 with the Gaussian observation error covariance being $\mathbf{R} = \mathbf{I}_{150}$.

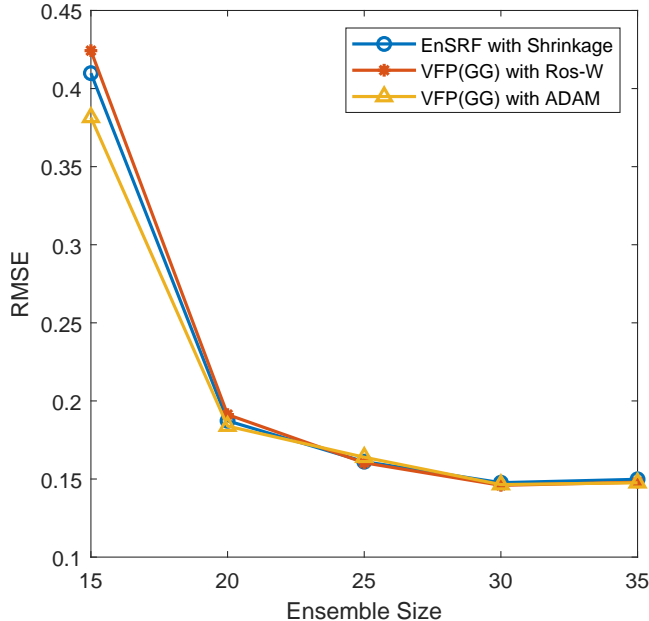


Fig. 7.5: A comparison of a shrinkage-based ensemble Kalman filter with the shrinkage-based VFP(GG) algorithm for the quasi-geostrophic equations. The VFP solution is obtained by two time-stepping algorithms, the IMEX Rosenbrock Euler-Maruyama, and the ADAM stochastic optimization scheme. As usual, ensemble size N is compared to the analysis RMSE.

We perform assimilation with our method VFP(GG) with RBLW shrinkage on the covariance estimates. We also wish to compare the performance of the time stepping procedure introduced in [Theorem 3.3](#) to that of the ADAM stochastic optimization procedure (see [Remark 6](#)). [subsection 7.3](#) shows that the VFP methods show similar performance compared to a shrinkage based left transform ensemble square root filter [\[5\]](#).

8. Conclusions. This work demonstrates a generalized framework to perform ensemble variational data assimilation subsuming several methods that have been developed over the past few years such as Langevin flow filter, mapping particle filter [\[42\]](#) and the particle flow filter [\[22\]](#). The variational Fokker-Planck method combines a deterministic drift that drives the ensemble to the analysis with a suitably chosen stochastic diffusion to ensure ensemble spread. The deterministic drift is calculated to minimize the Kullback-Leibler divergence between the intermediate ensemble i.e the ensemble that is moving from the prior to the analysis under the said Itô process. Our formulation allows for flexibility in the choice of distributions while at the same time, competing with state-of-the-art methods such as the various ensemble and variational methods. Our generalized approach combines the ideas of Fokker-Planck-based data assimilation [\[47\]](#) with assumed distributions on the ensemble. The said distributions make an assumption on their form whose parameters are chosen based on ensemble statistics. We also extend the idea of variational Fokker-Planck filtering to variational Fokker-Planck smoothing, and show that this approach is comparable to

state-of-the-art smoothing methods. To explicitly prevent ensemble collapse or filter divergence, we derive a regularization term that accounts for particle interactions via minimization of mutual information between particles. To evolve the Itô process corresponding to the system states, we devise a linearly-implicit-explicit scheme, namely the Rosenbrock-Euler-Maruyama, which has a strong order of half while at the same time, exhibiting good stability property by allowing larger time steps in the process evolution. The linearly-implicit Rosenbrock-Euler method provides a balance between the stable but expensive implicit Euler versus the cheap but unstable explicit Euler methods. We show that our methodology works well on low-dimensional systems such as the Lorenz '63 equations while at the same time, feasible at higher dimensional systems with localization and covariance shrinkage for the Lorenz '96 equations and quasi-geostrophic equations respectively.

One drawback of this method is that is the difficulty in choosing a parameterized distribution for the background and intermediate that is more faithful to particle filtering philosophy. This requires working with mixture distributions requiring elaborate parameterizations and tuning. Another drawback is that high dimensional problems are not flexible with arbitrary choices of the parameterized distributions, and only worked well with Gaussian assumptions. Though the derived linearly-implicit Rosenbrock-Euler-Maruyama method allows for larger timesteps than fully explicit methods, it is computationally expensive for realistic problems and requires further research to balance computational time, and fast convergence. Another interesting direction we intend to explore in a future work is using momentum methods to evolve the Itô process.

Acknowledgements. We thank Dr.David Higdon for useful discussions on statistics.

REFERENCES

- [1] M. ABRAMOWITZ, I. A. STEGUN, AND R. H. ROMER, *Handbook of mathematical functions with formulas, graphs, and mathematical tables*, American Journal of Physics, 56 (1988), pp. 958–958, <https://doi.org/10.1119/1.15378>, <https://doi.org/10.1119/1.15378>, <https://arxiv.org/abs/https://doi.org/10.1119/1.15378>.
- [2] W. ACEVEDO, J. DE WILJES, AND S. REICH, *Second-order accurate ensemble transform particle filters*, SIAM Journal on Scientific Computing, 39 (2017), pp. A1834–A1850, <https://doi.org/10.1137/16M1095184>, <https://doi.org/10.1137/16M1095184>, <https://arxiv.org/abs/https://doi.org/10.1137/16M1095184>.
- [3] J. L. ANDERSON, *A marginal adjustment rank histogram filter for non-gaussian ensemble data assimilation*, Monthly Weather Review, 148 (01 Aug. 2020), pp. 3361 – 3378, <https://doi.org/10.1175/MWR-D-19-0307.1>, <https://journals.ametsoc.org/view/journals/mwre/148/8/mwrD190307.xml>.
- [4] J. L. ANDERSON, *Exploring the need for localization in ensemble data assimilation using a hierarchical ensemble filter*, Physica D: Nonlinear Phenomena, 230 (2007), pp. 99–111, <https://doi.org/https://doi.org/10.1016/j.physd.2006.02.011>, <https://www.sciencedirect.com/science/article/pii/S0167278906002168>. Data Assimilation.
- [5] M. ASCH, M. BOCQUET, AND M. NODET, *Data Assimilation*, Society for Industrial and Applied Mathematics, Philadelphia, PA, 2016, <https://doi.org/10.1137/1.9781611974546>, <https://epubs.siam.org/doi/abs/10.1137/1.9781611974546>, <https://arxiv.org/abs/https://epubs.siam.org/doi/pdf/10.1137/1.9781611974546>.
- [6] K. BERGEMANN AND S. REICH, *A localization technique for ensemble kalman filters*, Quarterly Journal of the Royal Meteorological Society, 136 (2010), pp. 701–707, <https://doi.org/https://doi.org/10.1002/qj.591>, <https://rmets.onlinelibrary.wiley.com/doi/abs/10.1002/qj.591>, <https://arxiv.org/abs/https://rmets.onlinelibrary.wiley.com/doi/pdf/10.1002/qj.591>.
- [7] G. BURGERS, P. J. VAN LEEUWEN, AND G. EVENSEN, *Analysis scheme in the ensemble kalman filter*, Monthly Weather Review, 126 (1998), pp. 1719 – 1724, [https://doi.org/10.1175/1520-0493\(1998\)126\(1719:ASITEK\)2.0.CO;2](https://doi.org/10.1175/1520-0493(1998)126(1719:ASITEK)2.0.CO;2), <https://journals.ametsoc.org/view/>

- [journals/mwre/126/6/1520-0493.1998.126.1719_asitek.2.0.co.2.xml](https://doi.org/10.1175/1520-0493.1998.126.1719_asitek.2.0.co.2.xml).
- [8] Y. CHEN, A. WIESEL, Y. C. ELДАР, AND A. O. HERO, *Shrinkage Algorithms for MMSE Covariance Estimation*, IEEE Transactions on Signal Processing, 58 (2010), pp. 5016–5029, <https://doi.org/10.1109/TSP.2010.2053029>.
- [9] N. CHUSTAGULPROM, S. REICH, AND M. REINHARDT, *A hybrid ensemble transform particle filter for nonlinear and spatially extended dynamical systems*, SIAM/ASA Journal on Uncertainty Quantification, 4 (2016), pp. 592–608, <https://doi.org/10.1137/15M1040967>, <https://doi.org/10.1137/15M1040967>, <https://arxiv.org/abs/https://doi.org/10.1137/15M1040967>.
- [10] COMPUTATIONAL SCIENCE LABORATORY, *ODE test problems*, 2021, <https://github.com/ComputationalScienceLaboratory/ODE-Test-Problems> (accessed 2021-08-27).
- [11] T. M. COVER, *Elements of information theory*, John Wiley & Sons, 1999.
- [12] F. DAUM AND J. HUANG, *Particle flow for nonlinear filters*, in 2011 IEEE International Conference on Acoustics, Speech and Signal Processing (ICASSP), 2011, pp. 5920–5923, <https://doi.org/10.1109/ICASSP.2011.5947709>.
- [13] J. DORMAND AND P. PRINCE, *A family of embedded Runge-Kutta formulae*, Journal of Computational and Applied Mathematics, 6 (1980), pp. 19–26, [https://doi.org/https://doi.org/10.1016/0771-050X\(80\)90013-3](https://doi.org/https://doi.org/10.1016/0771-050X(80)90013-3), <https://www.sciencedirect.com/science/article/pii/0771050X80900133>.
- [14] L. C. EVANS, *An introduction to stochastic differential equations*, vol. 82, American Mathematical Soc., 2012.
- [15] G. EVENSEN, *Sequential data assimilation with a nonlinear quasi-geostrophic model using monte carlo methods to forecast error statistics*, Journal of Geophysical Research: Oceans, 99 (1994), pp. 10143–10162, <https://doi.org/https://doi.org/10.1029/94JC00572>, <https://agupubs.onlinelibrary.wiley.com/doi/abs/10.1029/94JC00572>, <https://arxiv.org/abs/https://agupubs.onlinelibrary.wiley.com/doi/pdf/10.1029/94JC00572>.
- [16] G. EVENSEN, *The Ensemble Kalman Filter: theoretical formulation and practical implementation*, Ocean Dynamics, 53 (2003), pp. 343–367, <https://doi.org/10.1007/s10236-003-0036-9>.
- [17] G. EVENSEN AND P. J. VAN LEEUWEN, *An ensemble kalman smoother for nonlinear dynamics*, Monthly Weather Review, 128 (2000), pp. 1852 – 1867, [https://doi.org/10.1175/1520-0493\(2000\)128<1852:AEKSFN>2.0.CO;2](https://doi.org/10.1175/1520-0493(2000)128<1852:AEKSFN>2.0.CO;2), https://journals.ametsoc.org/view/journals/mwre/128/6/1520-0493.2000.128.1852_aeksf.2.0.co.2.xml.
- [18] A. GARBUNO-INIGO, F. HOFFMANN, W. LI, AND A. M. STUART, *Interacting langevin diffusions: Gradient structure and ensemble kalman sampler*, SIAM Journal on Applied Dynamical Systems, 19 (2020), pp. 412–441, <https://doi.org/10.1137/19M1251655>, <https://doi.org/10.1137/19M1251655>, <https://arxiv.org/abs/https://doi.org/10.1137/19M1251655>.
- [19] G. GASPARI AND S. E. COHN, *Construction of correlation functions in two and three dimensions*, Quarterly Journal of the Royal Meteorological Society, 125 (1999), pp. 723–757, <https://doi.org/https://doi.org/10.1002/qj.49712555417>, <https://rmets.onlinelibrary.wiley.com/doi/abs/10.1002/qj.49712555417>, <https://arxiv.org/abs/https://rmets.onlinelibrary.wiley.com/doi/pdf/10.1002/qj.49712555417>.
- [20] T. M. HAMILL, *Interpretation of rank histograms for verifying ensemble forecasts*, Monthly Weather Review, 129 (2001), pp. 550 – 560, [https://doi.org/10.1175/1520-0493\(2001\)129<0550:IORHFV>2.0.CO;2](https://doi.org/10.1175/1520-0493(2001)129<0550:IORHFV>2.0.CO;2), https://journals.ametsoc.org/view/journals/mwre/129/3/1520-0493.2001.129.0550_iorhfv.2.0.co.2.xml.
- [21] T. HASTIE, R. TIBSHIRANI, AND J. FRIEDMAN, *The Elements of Statistical Learning: Data Mining, Inference, and Prediction*, Springer series in statistics, Springer, 2001, <https://books.google.com/books?id=VRzITwgNV2UC>.
- [22] C.-C. HU AND P. J. VAN LEEUWEN, *A particle flow filter for high-dimensional system applications*, Quarterly Journal of the Royal Meteorological Society, 147 (2021), pp. 2352–2374, <https://doi.org/https://doi.org/10.1002/qj.4028>, <https://rmets.onlinelibrary.wiley.com/doi/abs/10.1002/qj.4028>, <https://arxiv.org/abs/https://rmets.onlinelibrary.wiley.com/doi/pdf/10.1002/qj.4028>.
- [23] Y. HU, *Semi-implicit euler-maruyama scheme for stiff stochastic equations*, in Stochastic Analysis and Related Topics V, H. Korezlioglu, B. Øksendal, and A. S. Ustunel, eds., Boston, MA, 1996, Birkhäuser Boston, pp. 183–202.
- [24] B. R. HUNT, E. J. KOSTELICH, AND I. SZUNYOGH, *Efficient data assimilation for spatiotemporal chaos: A local ensemble transform kalman filter*, Physica D: Nonlinear Phenomena, 230 (2007), pp. 112–126.
- [25] M. A. IGLESIAS, K. J. LAW, AND A. M. STUART, *Ensemble kalman methods for inverse problems*, Inverse Problems, 29 (2013), p. 045001.

- [26] R. JORDAN, D. KINDERLEHRER, AND F. OTTO, *The variational formulation of the Fokker-Planck equation*, SIAM Journal on Mathematical Analysis, 29 (1998), pp. 1–17, <https://doi.org/10.1137/S0036141096303359>, <https://doi.org/10.1137/S0036141096303359>, <https://arxiv.org/abs/https://doi.org/10.1137/S0036141096303359>.
- [27] D. P. KINGMA AND J. BA, *Adam: A method for stochastic optimization*, arXiv preprint arXiv:1412.6980, (2014).
- [28] P. KLOEDEN AND E. PLATEN, *Numerical Solution of Stochastic Differential Equations*, Stochastic Modelling and Applied Probability, Springer Berlin Heidelberg, 2011, <https://books.google.com/books?id=BCvtssom1CMC>.
- [29] A. KOLMOGOROFF, *Über die analytischen methoden in der wahrscheinlichkeitsrechnung*, Mathematische Annalen, 104 (1931), pp. 415–458.
- [30] S. KOTZ, T. KOZUBOWSKI, AND K. PODGÓRSKI, *The Laplace distribution and generalizations: a revisit with applications to communications, economics, engineering, and finance*, no. 183, Springer Science & Business Media, 2001.
- [31] S. KULLBACK AND R. A. LEIBLER, *On information and sufficiency*, The annals of mathematical statistics, 22 (1951), pp. 79–86.
- [32] Q. LIU, *Stein variational gradient descent as gradient flow*, in Advances in Neural Information Processing Systems, I. Guyon, U. V. Luxburg, S. Bengio, H. Wallach, R. Fergus, S. Vishwanathan, and R. Garnett, eds., vol. 30, Curran Associates, Inc., 2017, <https://proceedings.neurips.cc/paper/2017/file/17ed8abedc255908be746d245e50263a-Paper.pdf>.
- [33] Q. LIU AND D. WANG, *Stein variational gradient descent: A general purpose bayesian inference algorithm*, in Proceedings of the 30th International Conference on Neural Information Processing Systems, NIPS’16, Red Hook, NY, USA, 2016, Curran Associates Inc., pp. 2378–2386.
- [34] E. LORENZ, *Predictability: a problem partly solved*, in Seminar on Predictability, 4-8 September 1995, vol. 1, Shinfield Park, Reading, 1995, ECMWF, ECMWF, pp. 1–18, <https://www.ecmwf.int/node/10829>.
- [35] E. N. LORENZ, *Deterministic nonperiodic flow*, Journal of Atmospheric Sciences, 20 (1963), pp. 130 – 141, [https://doi.org/10.1175/1520-0469\(1963\)020\(0130:DNF\)2.0.CO;2](https://doi.org/10.1175/1520-0469(1963)020(0130:DNF)2.0.CO;2), https://journals.ametsoc.org/view/journals/atsc/20/2/1520-0469_1963_020_0130_dnf_2_0_co_2.xml.
- [36] D. MAOUTSA, S. REICH, AND M. OPPER, *Interacting particle solutions of fokker-planck equations through gradient-log-density estimation*, Entropy (Basel, Switzerland), 22 (2020), p. 802, <https://doi.org/10.3390/e22080802>, <https://pubmed.ncbi.nlm.nih.gov/33286573>.
- [37] N. NÜSKEN AND S. REICH, *Note on interacting langevin diffusions: Gradient structure and ensemble kalman sampler by garbuno-inigo, hoffmann, li and stuart*, Tech. Report Arxiv: 1908.10890, University of Potsdam, 2019.
- [38] B. O’NEILL, *Exchangeability, correlation, and bayes’ effect*, International Statistical Review / Revue Internationale de Statistique, 77 (2009), pp. 241–250, <http://www.jstor.org/stable/27919725>.
- [39] A. A. POPOV AND A. SANDU, *A bayesian approach to multivariate adaptive localization in ensemble-based data assimilation with time-dependent extensions*, Nonlinear Processes in Geophysics, 26 (2019), pp. 109–122.
- [40] A. A. POPOV AND A. SANDU, *An explicit probabilistic derivation of inflation in a scalar ensemble kalman filter for finite step, finite ensemble convergence*, 2020, <https://arxiv.org/abs/2003.13162>.
- [41] A. A. POPOV, A. N. SUBRAHMANYA, AND A. SANDU, *A stochastic covariance shrinkage approach to particle rejuvenation in the ensemble transform particle filter*, Nonlinear Processes in Geophysics Discussions, (2021), pp. 1–14.
- [42] M. PULIDO AND P. J. VAN LEEUWEN, *Sequential Monte Carlo with kernel embedded mappings: The mapping particle filter*, Journal of Computational Physics, 396 (2019), pp. 400–415, <https://doi.org/https://doi.org/10.1016/j.jcp.2019.06.060>, <https://www.sciencedirect.com/science/article/pii/S0021999119304681>.
- [43] M. PULIDO AND P. J. VAN LEEUWEN, *Sequential Monte Carlo with kernel embedded mappings: The mapping particle filter*, Journal of Computational Physics, 396 (2019), pp. 400–415, <https://doi.org/https://doi.org/10.1016/j.jcp.2019.06.060>, <https://www.sciencedirect.com/science/article/pii/S0021999119304681>.
- [44] V. RAO, A. SANDU, M. NG, AND E. D. NINO-RUIZ, *Robust data assimilation using L1 and huber norms*, SIAM Journal on Scientific Computing, 39 (2017), pp. B548–B570.
- [45] S. REICH, *A gaussian-mixture ensemble transform filter*, Quarterly Journal of the Royal Meteorological Society, 138 (2012), pp. 222–233, <https://doi.org/https://doi.org/10.1002/qj.898>, <https://rmets.onlinelibrary.wiley.com/doi/abs/10.1002/qj.898>, <https://arxiv.org/>

- [abs/https://rmets.onlinelibrary.wiley.com/doi/pdf/10.1002/qj.898](https://rmets.onlinelibrary.wiley.com/doi/pdf/10.1002/qj.898).
- [46] S. REICH AND C. COTTER, *Probabilistic forecasting and Bayesian data assimilation*, Cambridge University Press, 2015.
 - [47] S. REICH AND S. WEISSMANN, *Fokker–planck particle systems for bayesian inference: Computational approaches*, SIAM/ASA Journal on Uncertainty Quantification, 9 (2021), pp. 446–482, <https://doi.org/10.1137/19M1303162>, <https://doi.org/10.1137/19M1303162>, <https://arxiv.org/abs/https://doi.org/10.1137/19M1303162>.
 - [48] S. ROBERTS, A. A. POPOV, A. SARSHAR, AND A. SANDU, *Ode test problems: a matlab suite of initial value problems*, arXiv preprint arXiv:1901.04098, (2021).
 - [49] Y. SAAD AND M. H. SCHULTZ, *Gmres: A generalized minimal residual algorithm for solving nonsymmetric linear systems*, SIAM Journal on scientific and statistical computing, 7 (1986), pp. 856–869.
 - [50] S. R. SAHANI PATHIRAJA, *Discrete gradients for computational Bayesian inference*, Journal of Computational Dynamics, 6 (2019), pp. 385–400.
 - [51] O. SAN AND T. ILIESCU, *A stabilized proper orthogonal decomposition reduced-order model for large scale quasigeostrophic ocean circulation*, Advances in Computational Mathematics, 41 (2015), pp. 1289–1319, <https://doi.org/10.1007/s10444-015-9417-0>, <https://doi.org/10.1007/s10444-015-9417-0>.
 - [52] A. TAGHVAEI AND P. MEHTA, *Accelerated flow for probability distributions*, in Proceedings of the 36th International Conference on Machine Learning, K. Chaudhuri and R. Salakhutdinov, eds., vol. 97 of Proceedings of Machine Learning Research, PMLR, 09–15 Jun 2019, pp. 6076–6085, <https://proceedings.mlr.press/v97/taghvaei19a.html>.
 - [53] P. TANDEO, P. AILLIOT, J. RUIZ, A. HANNART, B. CHAPRON, A. CUZOL, V. MONBET, R. EASTON, AND R. FABLET, *Combining analog method and ensemble data assimilation: Application to the lorenz-63 chaotic system*, in Machine Learning and Data Mining Approaches to Climate Science, V. Lakshmanan, E. Gilleland, A. McGovern, and M. Tingley, eds., Cham, 2015, Springer International Publishing, pp. 3–12.
 - [54] P. TRANQUILLI, S. R. GLANDON, A. SARSHAR, AND A. SANDU, *Analytical Jacobian-vector products for the matrix-free time integration of partial differential equations*, Journal of Computational and Applied Mathematics, 310 (2017), pp. 213–223, <https://doi.org/https://doi.org/10.1016/j.cam.2016.05.002>, <https://www.sciencedirect.com/science/article/pii/S0377042716302199>. Numerical Algorithms for Scientific and Engineering Applications.
 - [55] D. L. VAN KEKEM, *Dynamics of the lorenz-96 model: Bifurcations, symmetries and waves*, (2018).
 - [56] P. VAN LEEUWEN, *Particle filtering in geophysical systems*, Monthly Weather Review, 137 (2009), pp. 4089–4114.
 - [57] P. J. VAN LEEUWEN, H. R. KÜNSCH, L. NERGER, R. POTTHAST, AND S. REICH, *Particle filters for high-dimensional geoscience applications: A review*, Quarterly Journal of the Royal Meteorological Society, 145 (2019), pp. 2335–2365, <https://doi.org/https://doi.org/10.1002/qj.3551>, <https://rmets.onlinelibrary.wiley.com/doi/abs/10.1002/qj.3551>, <https://arxiv.org/abs/https://rmets.onlinelibrary.wiley.com/doi/pdf/10.1002/qj.3551>.
 - [58] R. VERSHYNIN, *High-dimensional probability: An introduction with applications in data science*, vol. 47, Cambridge university press, 2018.